nature portfolio

Peer Review File

Soft-matter multistate ionic neuromorphic processing based on cascade-heterointerfacial ion-traps

Corresponding Author: Professor Ziguang Zhao

This file contains all reviewer reports in order by version, followed by all author rebuttals in order by version.

Attachments originally included by the reviewers as part of their assessment can be found at the end of this file.

Version 0:

Reviewer comments:

Reviewer #2

(Remarks to the Author)
Nanofluidics typically rely on nanoscale confinement, which limits flexible ion control and scalability. This work introduces a gel-multiphasic ion transporter (GIT) that employs cascade heterointerfacial ion-traps to achieve low-power, multistate ionic neuromorphic functions. Graded electrostatic and steric interactions across its interfaces create hierarchical ion-retardation effects, enabling bidirectional rectification exceeding 10^3 and dual-order plasticity dependent on spike strength and timing. Importantly, memory phenomena emerge at ultralow voltages in the millivolt regime. The system supports both short- and long-term memory, as well as Hebbian, anti-Hebbian, and BCM learning. The authors further interface a GIT-based neuro-iontronic processor with a rat sciatic nerve, demonstrating biologically driven ionic neuromorphic processing and plasticity modulation. Conceptually, the manuscript is interesting; however, several unclear aspects currently limit its justification for publication in its present form. More specifically:

1. The reported phenomena are attributed to alternating ionic barriers, and the authors provide a theoretical framework to support this interpretation. However, there is no solid experimental validation of these barrier-dependent mechanisms. In principle, one would expect quantitative extraction of activation energies or equivalent energetic parameters governing ion transport, yet such analysis is absent. This omission weakens the connection between the proposed theory and the experimental observations. Please provide more experimental evidence.

2. The claimed BCM behavior is not convincingly justified. The manuscript does not clearly explain why the observed frequency-dependent transitions should be interpreted as BCM-like learning, nor does it establish the mechanistic basis linking the device physics to the BCM framework.

3. The discussion of memory retention is insufficient. Although the authors report short- and long-term memory effects, a quantitative analysis in missing. Quantitative retention curves, timescale analysis, and evidence linking trap dynamics to sustained states are needed to substantiate the claimed memory behavior.

4. The experimental context of Fig. 4 is unclear both in the text and within the figure. From the provided panels, it cannot be determined whether the demonstrated nerve–device interaction was conducted in vivo, ex vivo, or under simulated or asynchronous stimulation. The figure does not supply sufficient labeling or methodological indicators to resolve this ambiguity. As a result, the interpretation of “bioneuron-driven neuromorphic processing” is difficult to evaluate. Clear annotation within the figure, as well as explicit clarification in the main text, is required to establish the experimental conditions and the validity of the claimed biological relevance.

Reviewer #3

(Remarks to the Author)
Reviewer comments:
In this paper, Wu et al. developed a unique iontronic device, termed the gel-multiphasic ion transporter (GIT), which demonstrated outstanding ionic memristive effects and operated at biointerfaces as a bioiontronic device for neuromorphic

processing (neural signal transmission). The work is an interesting extension of their previous work (Science 382, 559-565 (2023)), which elegantly used a cascade-heterogated biphasic gel (HBG) for ion selection and the modulation of biological activity. Here, the authors applied the HBG principles to the development of the GIT, which, in my opinion, is fundamentally a bipolar membrane heterojunction, i.e., an iontronic diode. Many iontronic diodes have been reported previously. However, the HBG structure in this work introduced new, intriguing properties to the field, including memristive effects, low energy consumption, and ion specificity. Further, the last biological application is mind-blowing (I will mention the problem with it later). Therefore, I appreciate the authors' endeavour and believe this work has significant potential impact. However, some major issues need to be addressed before acceptance.

Major issues:

1. Writing issue:

The ionic mechanism of the GIT is very obscure and difficult to understand. The writing in Sections 'Cascade-heterointerface-trap ion transmission' and 'Bidirectional ionic rectification' is abstruse and mouthful, and Figs. 1 to 3 are not clear for the mechanism explanation. Below are my detailed comments.

1.1 I understand the strong connection and breakthrough between this work and the previous HBG paper. However, not every reader is aware of the HBG, and Figure 1 does not clearly present basic information about the GIT. What are the material compositions of the HBG? How does an actual device look? Some information in the SI should be put there, or an extended data Figure at least. And virtual photos of the device should be presented.

1.2 I would remove the long paragraph in Section 'Cascade-heterointerface-trap ion transmission', starting from 'The heterointerface architectures established ionic cross-interface transfer energy barriers (ΔE)…' to the end of the paragraph. The content here serves as an introduction, but it largely overlaps with the information in the abstract without giving any new information. Further, the many compound words/terms are difficult to read, failing to convey the meanings behind.

1.3 The awkward terms include 'ionic cross-interface transfer energy barriers', 'cascade-heterointerface-traps governed ionic nonlinear transmission', 'asymmetric central interfacial charge accumulation', 'spike-strength/timing dependent dual-order (i.e., unipolar and bipolar) plasticity features', etc.

1.4 I strongly recommend replotting Fig. 1b to 1e to first divide the CV scan into multiple steps/regions and correlate the mechanistic schematics (1b) aside to give explanations. The same for Fig. 3a to c.

1.5 Many terms used in this manuscript are also misleading. 'bidirectional ionic rectification' does not make sense to me. Rectification in the context of iontronics means that only one direction of ionic current can pass, i.e., it behaves as a diode. The 'bidirectional' nullifies this term. Also, the same effect has been widely observed in biological nanopores and correlated dropletronic memristive devices (DOI: 10.1039/d5cs00580a). The authors should mention this and provide a discussion.

1.6 The term 'neuromorphic' has also been widely used in this manuscript. However, its meaning is imprecise. 'Memristive' is a better and more accepted replacement.

1.7 The paragraph that starts with 'As illustrated in Fig. 1b and Supplementary Fig. 2…' is essential but difficult to read. I strongly recommend a rewrite with clear words and shorter sentences.

2. Mechanisms:

My understanding of the GIT is that it comprises two oppositely charged HBGs and forms an iontronic diode structure. In addition to conventional iontronic diodes, the unique structure of the HBGs induces a significant capacitance effect at the center heterointerface, so-called the relay medium phase (RMP), which results in the memristive feature.

2.1 I don't understand why ΔEn > … > ΔE2 > ΔE1. The HBG is evenly distributed, and the cross-interface transfer energy barriers should be the same. Of course, their accumulation cascades, e.g., the working mechanism of HBG.

2.2 'Initially, AEP acted as a cation- and anion-enriched phase, while CEP contained free anions.' What do you mean? Shouldn't AEP only contain free cations?

2.3 The calculation of forward (f) and reverse (f') rectification ratios is unclear. The methods used in conventional iontronic diodes should be considered, and the performance under alternating voltages should be measured.

2.4 The influence of frequency and scanning rates should be further explained in the rectification section, and clearly shown in the Figures.

2.5 The part 'The GIT material was fabricated through a…' should be moved to the beginning.

2.6 The influence of various ion species is important. Could the authors try protons?

2.7 The mechanism of ion concentration is unclear. The results in SI Fig. 16 seem to show that higher ion concentration shows higher ion rectification, which is contradictory to the explanation in the main text.

2.8 The hydrogel materials (bilayer polyelectrolyte hydrogelCa/Al) should be clearly explained. Different hydrogel materials may provide different performances.

2.9 I don't understand the need to differentiate the unipolar and bipolar plasticity features. Isn't the unipolar state a part of the bipolar state?

2.10 The ultra-low energy consumption (0.61 pJ/spike) is an important claim of the authors. However, how is this defined? Is there a standard for the minimum weight change required for a single spike? Or how many spikes does the GIT need to achieve the maximal weight change? Basically, I assume the smaller the weight change per spike, the less energy it needs per spike. Moreover, how is the weight measured? What is the impedance of the total device? Will that affect energy consumption?

3. Biological experiments

The biological experiments are amazing. However, many questions exist, such as why use GITCa/Al not other ions? Why does the device have two channels and 4 electrodes? Biocompatibility issues. What happened at the biointerfaces? What endogenous neural signals are involved? These questions are important and worth further work (another paper) to fully explain. Therefore, I strongly recommend removing the bioapplication and only focusing on the memristive application.

4 Other issues

4.1 The authors should briefly explain how to use GITs as modular components, the miniaturisation, and how to integrate

them into iontronic systems.
4.2 Microfont in Fig. 4b. Time is unclear in SI Fig. 5. SI Fig. 15 is unclear. Can a single-sided GIT achieve a memristive effect? f Data in SI Fig. 19 is missing.

Version 1:

Reviewer comments:

Reviewer #2

(Remarks to the Author)
In the revised version of the manuscript, the authors addressed most of my comments. I believe that in this form, the manuscript id suitable for publication in Nature Electronics.

Reviewer #3

(Remarks to the Author)
Reviewer comments:
The authors have addressed my comments in a very complete manner. They have provided additional data where required, modified Figures, and enhanced parts of the discussion. I recommend acceptance for publication of this work in Nature Electronics.
Minor Comment:
1. Related to Figure 4, the definition and importance of interfacing biology with iontronic devices (bioiontronics) should be further discussed.
2. Small fonts still exist in some main Figures.

Responses to Referees' Comments

Reviewer 1

Nanofluidics typically rely on nanoscale confinement, which limits flexible ion control and scalability. This work introduces a gel-multiphasic ion transporter (GIT) that employs cascade heterointerfacial ion-traps to achieve low-power, multistate ionic neuromorphic functions. Graded electrostatic and steric interactions across its interfaces create hierarchical ion-retardation effects, enabling bidirectional rectification exceeding 10^3 and dual-order plasticity dependent on spike strength and timing. Importantly, memory phenomena emerge at ultralow voltages in the millivolt regime. The system supports both short- and long-term memory, as well as Hebbian, anti-Hebbian, and BCM learning. The authors further interface a GIT-based neuro-iontronic processor with a rat sciatic nerve, demonstrating biologically driven ionic neuromorphic processing and plasticity modulation. Conceptually, the manuscript is interesting; however, several unclear aspects currently limit its justification for publication in its present form. More specifically:

Response: We are sincerely grateful and deeply gratified by the reviewer's thoughtful evaluation and clear understanding of our work. According to your insightful and constructive suggestions, we have thoroughly revised both the manuscript and Supporting Information to strengthen the experimental evidence and technical details presented in our study.

Comment 1: *The reported phenomena are attributed to alternating ionic barriers, and the authors provide a theoretical framework to support this interpretation. However, there is no solid experimental validation of these barrier-dependent mechanisms. In principle, one would expect quantitative extraction of activation energies or equivalent energetic parameters governing ion transport, yet such analysis is absent. This omission weakens the connection between the proposed theory and the experimental observations. Please provide more experimental evidence.*

Response: We appreciate the reviewer's recognition of our theoretical analysis for interpreting cross-interface ionic transport barriers. We fully agree that quantitative experimental evidence is essential to validate the proposed cross-interface ionic transport barriers and the heterointerface-trap mechanism. To address this, we have performed two independent sets of experiments, including relaxation-time energy spectrum and ionic activation energy (E_a). These results provide direct experimental evidence for the proposed mechanism, which is entirely independent of the theoretical section.

To provide direct experimental evidence for the proposed cascaded-heterointerface-trap

mechanism, we perform relaxation-time energy spectrum measurements focusing on the center-heterointerface-related region (~5 μm) of the GIT systems under a dynamically applied electric field, where the bias is swept from 12 mV to 0 mV at a scan rate of 1 mV s^{-1}. During this process, the relaxation-time energy spectrum reveals the interfacial potential evolution and distribution behaviors of cations and anions, demonstrating the ionic accumulation and dissipation dynamics for the center-heterointerface-trap (***Fig. R1***). Under the applied electric field, Na^+ and Cl^- ions transport along the electric-field direction and gradually migrate toward opposite sides of the center-heterointerface. As a result, an asymmetric charge distribution progressively forms within the heterointerface region, generating a built-in positive potential aligned with the applied electric field. When the bias returns to zero and the field is removed, the accumulated heterointerface-trap becomes difficult to sustain, and the cations and anions begin to dissipate. This relaxation process occurs rapidly, and the asymmetric charge distribution collapses within a short time window (~12.2 s). The corresponding built-in potential simultaneously decreases to zero. This result also exhibits the hysteretic ionic transport behavior associated with the heterointerface-traps. Combining the theoretical section presented in the original manuscript, these results provide direct and strong evidence for the heterointerface-trap dynamics within the GIT systems.

In addition, we conduct ionic conductance measurements to quantitatively extract activation energies as an energetic parameter for ion cross-interface transmission. By analyzing the Arrhenius dependence of the ionic conductance under identical measurement conditions, the extracted E_a values show a clear distinction between the GIT, AEP, and CEP, with E_a = 32.8 kJ/mol for the GIT, compared with 15.4 kJ/mol for the AEP and 17.3 kJ/mol for the CEP (***Fig. R2***). In the single-phase AEP and CEP, ion transport occurs within a homogeneous polyelectrolyte network, where ions migrate primarily through bulk diffusion in a continuous hydrated matrix. In such homogeneous diffusion systems, the activation energy mainly reflects the energetic cost associated with ion transmission through the solvent environment and polyelectrolyte network, resulting in relatively low E_a values. In contrast, the substantially higher E_a in the GIT system provides a quantitative experimental signature of the additional energy penalty required to overcome the cascaded heterointerfacial energy barriers (ΔE) during cross-interface transmission. Therefore, it acts as important experimental evidence for the presence of the heterointerfacial energy barrier. Within the GIT systems, the gradient of cascaded cross-interface transfer energy barriers further induces dynamic heterointerface-trap effects.

We sincerely thank the reviewer for this valuable suggestion. In response, the relaxation-time

energy spectrum measurements have been added to the "Cascade-heterointerface-trap ion transmission" section, while the activation energy analysis has been incorporated into the "Ionic bipolarity rectification" section, significantly strengthening the experimental validation of the proposed cascade-heterointerface-traps governed ion transmission mechanism.

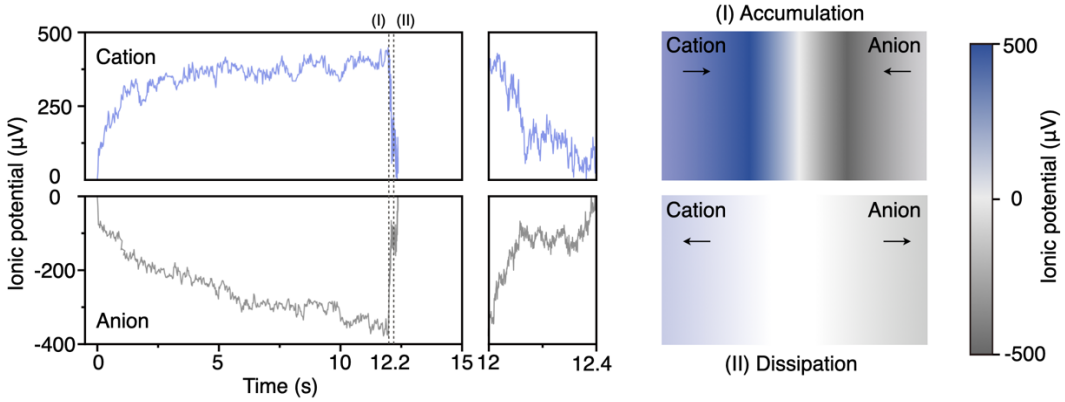

***Fig. R1* (new Supplementary Fig. 9)** *Relaxation-time energy spectrum for cross-interface ion transport of the center-heterointerface-related region (5 μm) within the GIT_{Na} systems, showing asymmetrical cationic and anionic interface distributions and the corresponding dynamic built-in potentials.*

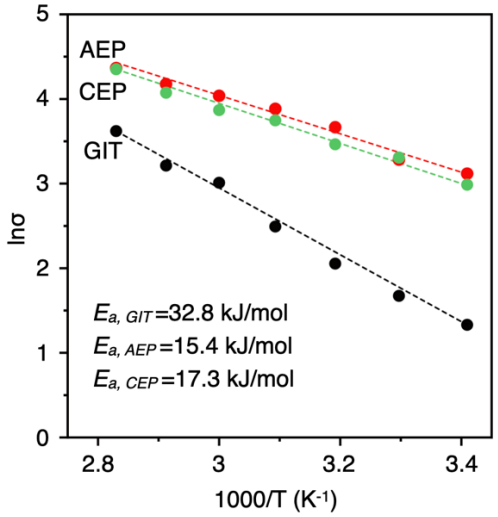

***Fig. R2* (new Supplementary Fig. 13)** *Activation energy measurements of mobile Na^+ and Cl^- ions in the GIT, AEP, and CEP.*

Comment 2: *The claimed BCM behavior is not convincingly justified. The manuscript does not clearly explain why the observed frequency-dependent transitions should be interpreted as BCM-like learning, nor does it establish the mechanistic basis linking the device physics to the BCM framework.*

Response: We appreciate the reviewer's insightful comment highlighting the need to more clearly

justify the BCM behavior and to establish the mechanistic connection between the device physics and the BCM learning framework. In the GIT systems, the construction and dissipation of cascade-heterointerface-traps occur on distinct temporal scales, making the ionic synaptic response strongly dependent on stimulation frequency, which is the fundamental requirement for implementing the BCM learning rule. We would explain how the frequency-dependent synaptic responses of the GIT systems relate to the BCM learning rule.

In our experiments, the stimulation frequency refers to the repetition rate of the applied electrical spikes used to emulate presynaptic activity, and is associated with memory time (t_r) effects. Specifically, a train of identical voltage pulses with different temporal intervals is applied to the $GIT_{Ca/Al}$, corresponding to frequencies ranging from 0.1 Hz to 1000 Hz. As shown in ***Fig. R3a***, the $GIT_{Ca/Al}$ systems with short-term and long-term memory effects exhibit clear frequency-dependent memory behavior originating from the temporal dynamics of cascaded-heterointerface-traps. Both short-term and long-term memory effects are suppressed at the lowest and highest frequency limits, where heterointerface-traps cannot be effectively constructed or are rapidly dissipated. These results demonstrate a direct correlation between stimulation frequency and the memory behavior of the GIT systems, establishing frequency as the effective activity variable, analogous to the neuronal firing rate in biological systems, which provides the requisite physical basis for BCM learning rule.

In the classical Bienenstock-Cooper-Munro (BCM) learning rule, synaptic modification is governed by the level of postsynaptic activity, which determines whether synaptic potentiation or depression occurs. Importantly, this activity is typically interpreted as the average firing rate of the postsynaptic neuron, and the transition between potentiation and depression is regulated by an activity-dependent modification threshold, which gives rise to the characteristic sliding-threshold behavior of BCM learning. A key prerequisite for establishing such an activity-dependent modification threshold is the coexistence and competition of synaptic potentiation and depression processes. In other words, the presence of both Hebbian and anti-Hebbian plasticity provides the necessary condition for implementing BCM-type learning. In our system, these complementary synaptic functions arise from two distinct GIT material configurations. For the $GIT_{Ca/Al}$ system, the Hebbian learning rule is faithfully implemented via spike-strength/timing-dependent plasticity. The conductance change ΔG is initially positive, indicating synaptic potentiation, and gradually decreases toward zero as $|\Delta t|$ increases, consistent with the classical temporal Hebbian profile. In contrast, by reprogramming the ionic composition of the CEP to Cl^-/ClO_4^-, the $GIT_{Cl/ClO}$ system exhibits a reversed learning profile,

consistently showing negative ΔG for both positive and negative Δt, indicating persistent synaptic depression irrespective of spike order.

In our system, by integrating these opposing ionic dynamics into a dual-crossbar architecture, the system's net synaptic weight change (ΔG) becomes a function of the frequency-dependent competition between the Hebbian $GIT_{Ca/Al}$ channel and the anti-Hebbian $GIT_{Cl/ClO}$ channel. The BCM learning rule is investigated by first setting different initial conductance states (G_O = 1, 2, and 3 μS) of the device and then sweeping the stimulation frequency. As shown in ***Fig. R3b***, the synaptic weight change (ΔG) exhibits a clear transition from depression (ΔG < 0) at low frequencies to potentiation (ΔG > 0) at higher frequencies. Crucially, we observe that the transition frequency, representing the modification threshold, systematically shifts from approximately 40 Hz to 70 Hz as G_O increases. When G_O is set to 3 μS, depression dominated by the anti-Hebbian $GIT_{Cl/ClO}$ channel prevails at low frequencies (< 40 Hz) because the long spike intervals suppress the Hebbian channel's conductance enhancement. Conversely, higher frequencies (> 70 Hz) lead to potentiation-dominated responses. This frequency-dependent competition, coupled with the observed shift in transition frequency, faithfully replicates the sliding-threshold dynamics essential to the BCM framework. We sincerely thank the reviewer for this valuable comment. The corresponding discussions have been added and further strengthened in the "Multistate ionic neuromorphics section" of the revised manuscript.

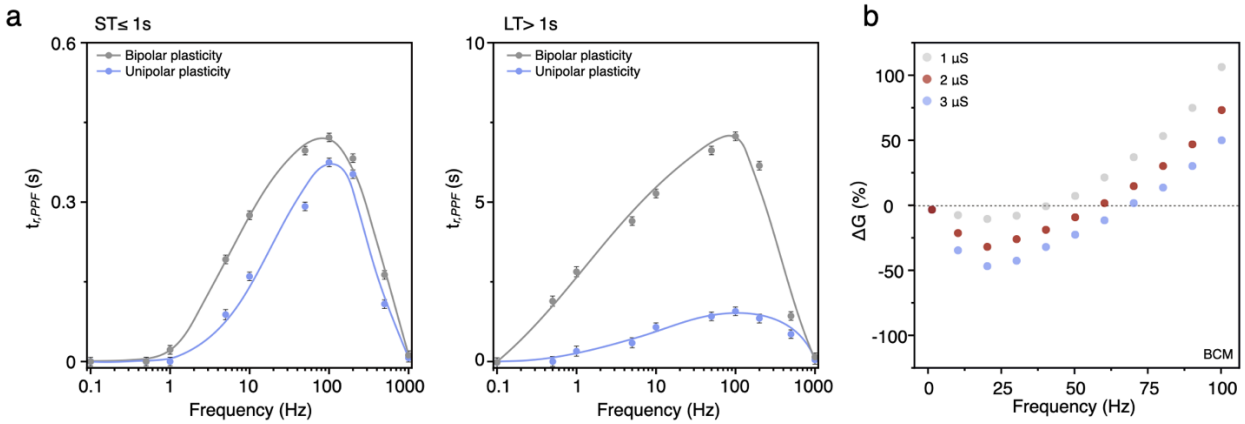

Fig. R3 ***a.*** *Paired-pulse facilitation retention time ($t_{r,PPF}$) of the $GIT_{Ca/Al}$ with short-/long-term memory under varying pulse frequencies ranging from 0.1 Hz to 1000 Hz.* ***b.*** *Integrating both $GIT_{Ca/Al}$ and $GIT_{Cl/ClO}$ into the dual-crossbar system, the BCM learning rule can be implemented. Under dynamic initial conductance conditions (G_O ranging from 1 to 3 μS), ΔG gradually shifts from negative to positive with increasing spike frequency, indicating a frequency-relevant transition from synaptic depression to potentiation.*

Comment 3: *The discussion of memory retention is insufficient. Although the authors report short- and long-term memory effects, a quantitative analysis in missing. Quantitative retention curves, timescale analysis, and evidence linking trap dynamics to sustained states are needed to substantiate the claimed memory behavior.*

Response: We appreciate the reviewer's insightful comment regarding the insufficient quantitative analysis of memory retention. Following the reviewer's suggestion, we have now expanded the memristive characterization by providing a more complete quantitative analysis of the retention dynamics in both the revised manuscript and the Supplementary Information.

We first quantify the temporal retention characteristics of the GIT system using paired-pulse measurements (***Fig. R4***). Representative paired-pulse ionic current responses under both positive and negative electric fields are shown for different ionic configurations, revealing clear paired-pulse facilitation (PPF) and paired-pulse depression (PPD) behaviors associated with short- and long-term time scale features (***Fig. R4a-4b***). Specifically, for the $GIT_{Ca/Al}$ systems with dual-order plasticity, the ionic current facilitation (Δi_{PPF}) values reach 26.8 nA and 33.9 nA in the short-term (ST) regime, and 39.8 nA and 52.1 nA in the long-term (LT) regime, under a paired-pulse interval of 10 ms (corresponding to a square-wave frequency of 100 Hz). From these measurements, we extract the paired-pulse retention time (t_r), defined as the characteristic time required for the facilitated or depressed postsynaptic ionic current to decay back to the baseline steady state after stimulation. As shown in ***Fig. R4c***, a statistical summary of the extracted retention times is provided, which clearly shows that bication configurations consistently exhibit longer retention times than monocation systems across both ST and LT regimes. This difference arises because distinct ionic configurations produce distinct effective ionic capacitances and therefore different memory behaviors. For the monocation configuration (GIT_{Ca}), the extracted t_r values reach 173.2 ms and 191.8 ms in the ST regime, and further extend to 0.62 s and 3.31 s in the LT regime. In contrast, when bication configurations are introduced ($GIT_{Ca/Al}$), the retention time is significantly prolonged, reaching 376.1 ms and 423.2 ms in ST, and further extends to 1.61 s and 7.14 s in LT. This difference arises because the coexistence of Ca^{2+} and Al^{3+} ions induces stronger cascade-heterointerface-trap formation and enhanced ionic accumulation, thereby slowing the dissipation of the cascade-heterointerface-trap and producing a larger extension of the retention time. In the revised ***Supplementary Fig. 29,*** we further present the memory retention time of the GIT_{Ca} and $GIT_{Ca/Al}$ systems under ten consecutive pulses.

Importantly, according to the reviewer's suggestion to strengthen the connection between

heterointerface-trap dynamics and memory behaviors, we have supplemented memristive hysteresis measurements and quantitatively analyzed the hysteresis loop areas of the $GIT_{Ca/Al}$ systems (***Fig. R5***). As shown in ***Fig. R5a-5b*** ***(new Supplementary Fig. 22a-22b)***, dual-order memristive hysteresis loops are obtained under both short-term (ST) and long-term (LT) stimulation conditions. The corresponding hysteresis loop areas are summarized in ***Fig. R5c*** ***(new Supplementary Fig. 22c)***. In the short-term regime, the loop area increases from 257.3 μV·A (1^{st}) to 357.1 μV·A (2^{nd}). Meanwhile, the long-term regime exhibits significantly larger loop areas, increasing from 420.3 μV·A (1^{st}) to 535.5 μV·A (2^{nd}). The hysteresis loop area reflects the strength of cascade-heterointerface-traps, which is closely associated with ionic accumulation and relaxation dynamics. Therefore, these results indicate a related memory retention behavior, governed by heterointerface-trap-regulated ion dynamics in the GIT systems. Moreover, we further update the results and discussions about the spike-strength-dependent and frequency-dependent features of GIT systems (***Fig. R6***). "***Supplementary Fig. 28*** exhibited detailed t_r values of the $GIT_{Ca/Al}$ across different frequency ranges from 0.1 Hz to 1000 Hz. The frequency-relevant t_r modulation derived from dynamic construction and dissipation of cascade-heterointerface-traps under different stimulus frequencies. The system demonstrated an optimal operational window approximately between 1 Hz and 100 Hz. Both short-term and long-term memory effects were suppressed at the lowest and highest frequency limits, where heterointerface-traps cannot be effectively constructed or are rapidly dissipated." And "Moreover, ***Fig. 3f*** and ***Supplementary Fig. 28*** exhibited the dependency between spike-strength and memory timescale effects of the GIT systems with different ST and LT features. Quantifying the dual-order plasticity factors (k) in the system, defined as the slope of t_r relative to spike voltage amplitude, presented the neuron-like shallow and deep degree of synaptic plasticity to input signal strengths. The k for the short-term regime ranged from 3.365 to 7.505, depending on the transition between unipolar and bipolar states. Contrastingly, for the LT features of the GIT, k increased significantly, reaching values up to 56.76 and 517.48. When the input amplitude dropped below approximately 18 mV, t_r decreased significantly below 1 s, clearly exhibiting the transition from LT to ST memory. These results quantitatively substantiate the multistate ionic neuromorphic capabilities of the GIT system, which are governed by spike-strength-dependent cascade-heterointerface-trap dynamics."

Together, in the new manuscript, the added results provide comprehensive quantitative evidence that the claimed time-scale memory behaviors arise from cascaded-heterointerface-traps in the GIT system.

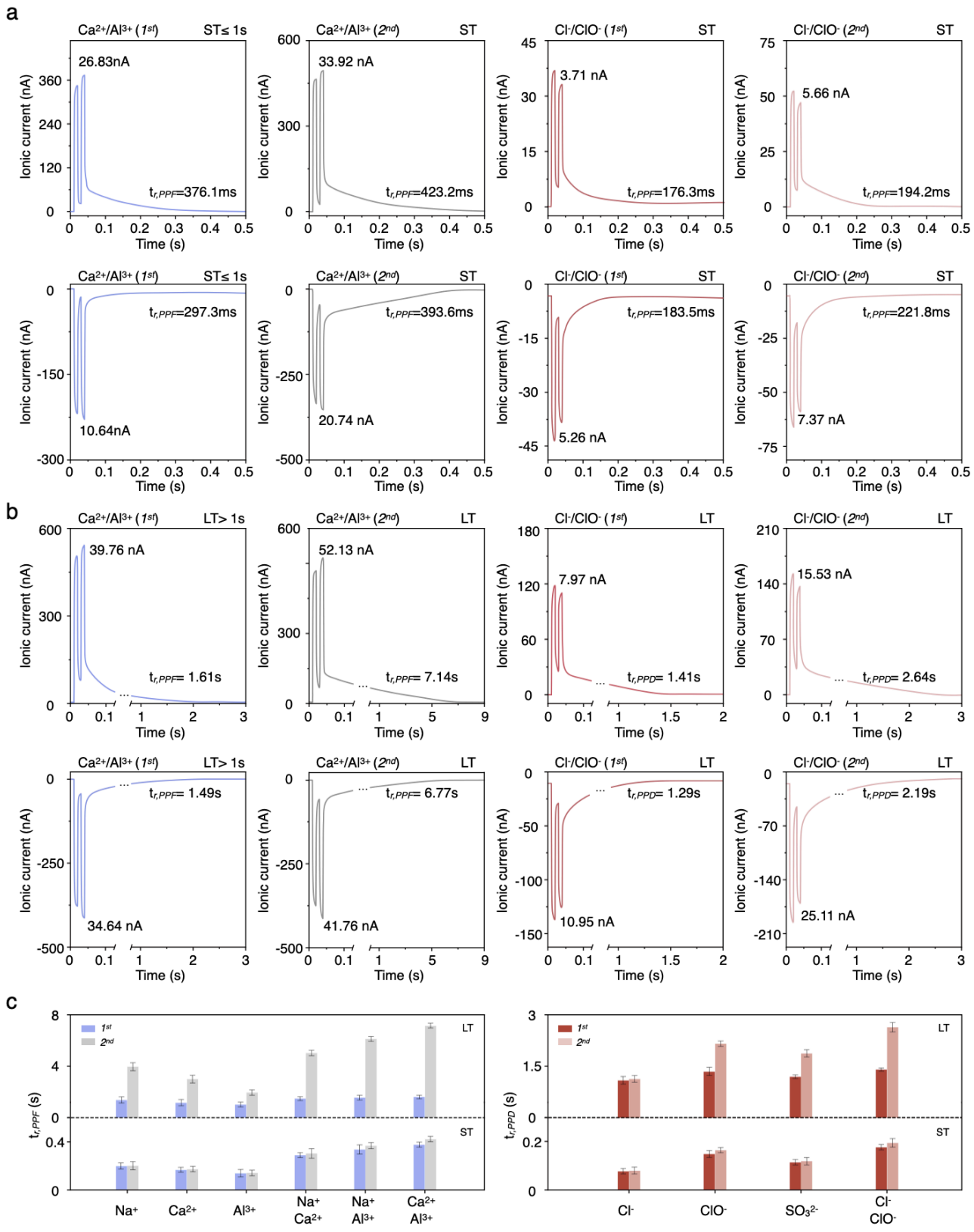

***Fig. R4* a-b (new Supplementary Fig. 27).** *Paired-pulse ionic current responses of the* $GIT_{Ca/Al}$ *and the*

$GIT_{Cl/ClO}$ with short-/long-term memory features under varying positive and negative electric field. ***c.*** *Paired-pulse facilitation retention time ($t_{r,PPF}$) and paired-pulse depression retention time ($t_{r,PPD}$) of GITs with varying ion configurations, governed by the dual-order plasticity and the timescale memristive effect.*

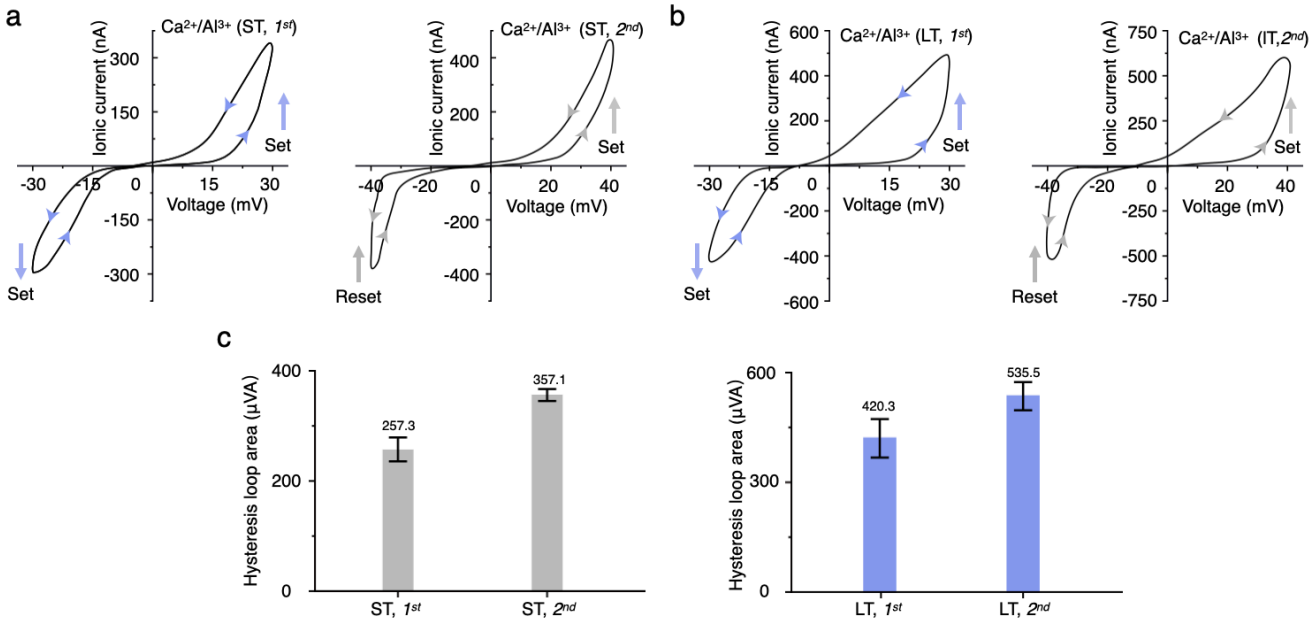

Fig. R5 ***(new Supplementary Fig. 22)*** *Dual-order I-V characteristic curves* ***(a-b)*** *and hysteresis loop area* ***(c)*** *of the $GIT_{Ca/Al}$ with short-/long-term memory features.*

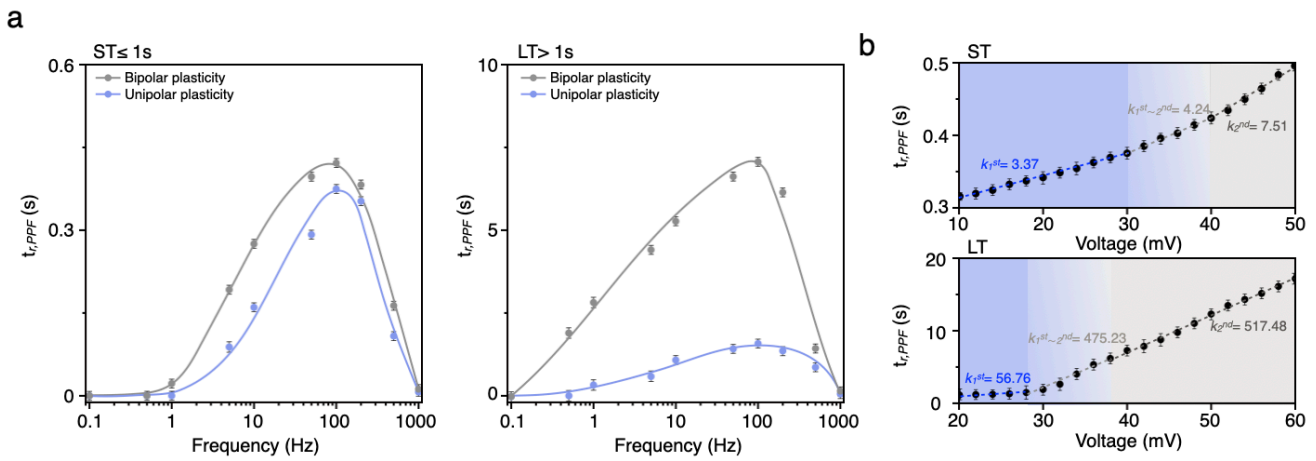

Fig. R6 ***a.*** *Paired-pulse facilitation retention time ($t_{r,PPF}$) of the $GIT_{Ca/Al}$ with short-/long-term memory under varying pulse frequencies ranging from 0.1 Hz to 1000 Hz.* ***b.*** *Dual-order plasticity factors (k) of the $GIT_{Ca/Al}$ with short-/long-term memory, respectively. k serves as the slope of t_r with respect to the amplitude of the spike voltage, exhibiting a metric for evaluating the degree of synaptic plasticity in the GIT system.*

***Comment 4:**. The experimental context of Fig. 4 is unclear both in the text and within the figure. From the provided panels, it cannot be determined whether the demonstrated nerve-device interaction was conducted in vivo, ex vivo, or under simulated or asynchronous stimulation. The figure does not supply sufficient labeling or methodological indicators to resolve this ambiguity. As a result, the interpretation of "bioneuron-driven neuromorphic processing" is difficult to evaluate. Clear annotation within the figure, as well as explicit clarification in the main text, is required to establish the experimental conditions and the validity of the claimed biological relevance.*

Response: We thank the reviewer for raising this important point regarding the experimental context of ***Fig. 4***. We would like to clarify that the biological experiments presented in ***Fig. 4*** are conducted *in vivo* using anesthetized rat models. The *in vivo* neuro-iontronic processor is directly interfaced with the transected sciatic nerve of the living animal to form a biohybrid neural circuit. It is important to note that the experimental setup does not involve an *ex vivo* neural-device interfacing system. The GIT-based device is also not driven by externally simulated electrical inputs delivered to biological nerves, nor is it intended as an illustration of signal simulation. Following the reviewer's suggestion, we have now explicitly clarified this information in ***Fig. R7*** ***(new Fig. 4)***, the corresponding figure caption, and the related discussions in the revised manuscript, with particular emphasis on the *in vivo* applications.

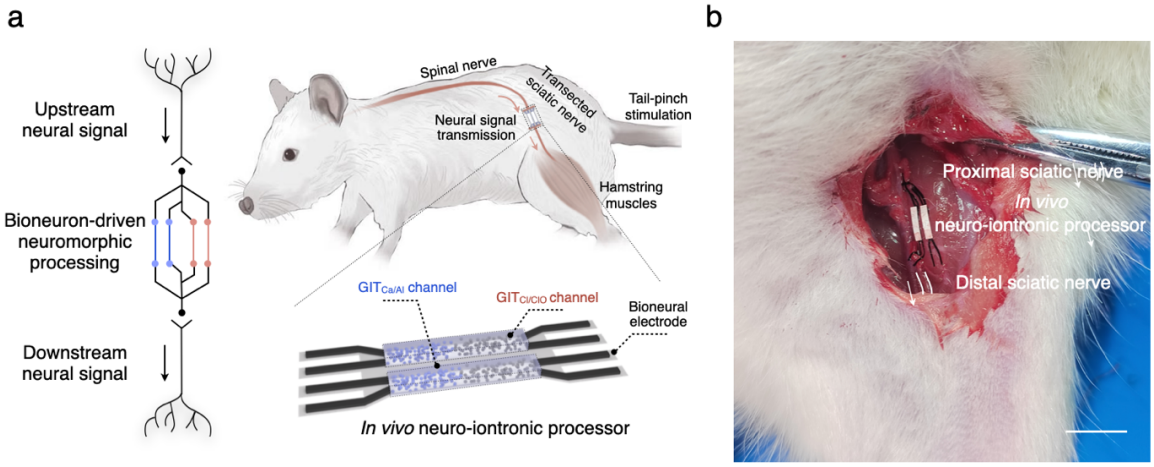

Fig. R7 ***(new Fig. 4a and 4c) a,*** *Schematic illustration of the in vivo neuro-iontronic processor integrated with GIT channels, constructing a biohybrid neural circuit. Driven by upstream endogenous neural potential spike signals, $GIT_{Ca/Al}$ and $GIT_{Cl/ClO}$ channels respectively exhibit neuromorphic potentiation and depression, originating from distinct cascade-heterointerface-traps ion transmission. Matching and interfacing with the rat's transected sciatic nerve, the in vivo neuro-iontronic processor*

reconfigures neural signal conduction and implements neural plasticity modulation. ***b,*** *Image of the biohybrid neural circuit with the in vivo neuro-iontronic processor interfacing the rat's transected sciatic nerve. Scale bar, 2.5 mm.*

The *in vivo* neuro-iontronic processor possesses intrinsic signal transduction and processing capabilities and can be embedded within the sciatic neural pathway. It actively modulates bioelectrical signals originating from the upstream nerve segment and relays the processed output to the downstream nerve terminals. Upstream neural activity generates extracellular bioelectrical activity that serves as input biopotential signals to the GIT processor, further activating heterointerface-trap dynamics and producing neuromorphic ionic currents. Thus, these neuromorphic signals can in turn modulate the distal nerve interface to facilitate and trigger action potentials in the downstream nerve. Importantly, we also conduct control experiments without the GIT processor, which yield no detectable downstream response, further confirming that the signal transmission across the transected nerve is entirely dependent on the functional integration of the GIT device. In this study, the GIT system features the intrinsic low-energy-consumption characteristics and establishes a functional biohybrid neural circuit for the processor's neuromorphic modulation within the neural communication pathway.

In addition, considering that the proposed GIT-based device is designed for *in vivo* neural interfacing, biocompatibility represents an important criterion for evaluating its potential biological applicability. Therefore, we have further included biocompatibility evaluations of GITs, which confirm the *in vivo* neuro-iontronic processor's minimal physiological impact (***Figs. R8-9***).

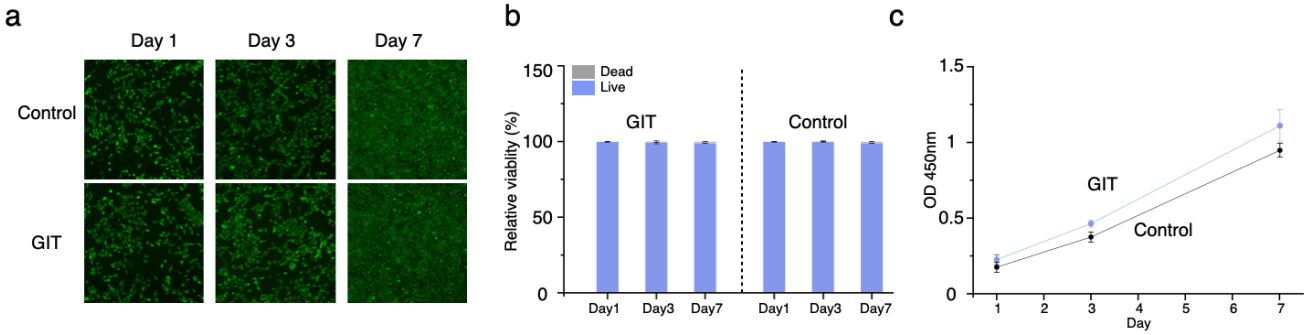

Fig. R8 ***(new Supplementary Fig. 34)*** *Live/dead fluorescence staining images show the changes in cell state on days 1, 3, and 7 of culture in the control and GIT-treated groups. Green fluorescence represents surviving cells. Both groups of cells exhibited good viability and continuous proliferation throughout the culture period, with cell density increasing significantly over time, forming a dense cell layer by day 7. Compared with the control group, no significant cytotoxicity or proliferation inhibition was observed in the GIT -treated group, indicating that the GIT system has good biocompatibility.*

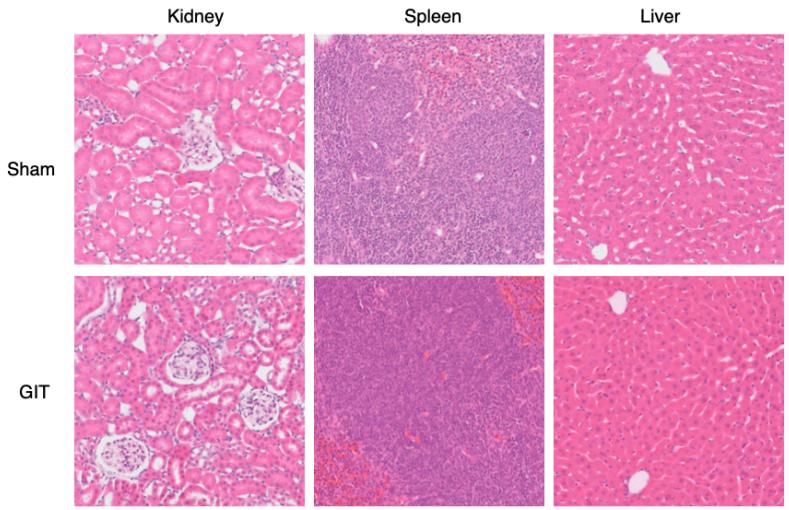

Fig. R9 ***(new Supplementary Fig. 35)*** *Representative H&E staining images of major organs (kidney, spleen, and liver) from rats in the sham-operated control group (Sham) and the gel-implanted group (GIT). Scale bar:100μm. n=6.*

Again, we sincerely appreciate the reviewer for this constructive comment and for the opportunity to further strengthen our work. We fully acknowledge the reviewer's concern that the mechanistic discussion, BCM learning rule, and in vivo biological application may have appeared speculative in the previous version of our manuscript. In response, a comprehensive revision is undertaken to significantly strengthen the experimental evidence and improve the interpretations and discussions. We believe that the manuscript has been significantly strengthened and is now suitable for acceptance.

Reviewer 2

In this paper, Wu et al. developed a unique iontronic device, termed the gel-multiphasic ion transporter (GIT), which demonstrated outstanding ionic memristive effects and operated at biointerfaces as a bioiontronic device for neuromorphic processing (neural signal transmission). The work is an interesting extension of their previous work (Science 382, 559-565 (2023)), which elegantly used a cascade-heterogated biphasic gel (HBG) for ion selection and the modulation of biological activity. Here, the authors applied the HBG principles to the development of the GIT, which, in my opinion, is fundamentally a bipolar membrane heterojunction, i.e., an iontronic diode. Many iontronic diodes have been reported previously. However, the HBG structure in this work introduced new, intriguing properties to the field, including memristive effects, low energy consumption, and ion specificity. Further, the last biological application is mind-blowing (I will mention the problem with it later). Therefore, I appreciate the authors' endeavour and believe this work has significant potential impact. However, some major issues need to be addressed before acceptance.

Response: We sincerely appreciate the reviewer for the positive evaluation of our manuscript, including the recognition of its novelty, structural clarity, and relevance to the field of iontronic neuromorphic systems. Your constructive comments have helped us further improve the manuscript. Detailed point-by-point responses are provided below.

Comment 1-1: *The ionic mechanism of the GIT is very obscure and difficult to understand. The writing in Sections 'Cascade-heterointerface-trap ion transmission' and 'Bidirectional ionic rectification' is abstruse and mouthful, and Figs. 1 to 3 are not clear for the mechanism explanation.*

Below are my detailed comments. I understand the strong connection and breakthrough between this work and the previous HBG paper. However, not every reader is aware of the HBG, and Figure 1 does not clearly present basic information about the GIT. What are the material compositions of the HBG? How does an actual device look? Some information in the SI should be put there, or an extended data Figure at least. And virtual photos of the device should be presented.

Response: We sincerely thank the reviewer for the constructive suggestions. According to the reviewer's comments, we have revised the relevant mechanistic details presented in ***Figs. 1-3***. In the revised manuscript, we have provided fundamental information, including material compositions and real photographs of the GIT system. The ***Fig. R10*** ***(new Fig. 1)*** exhibits the real photographs of the GIT system. We also have deleted the original statement and rewritten a new paragraph at the beginning

of the Results and Discussion section, providing a clearer introduction to the preparation and characterization of the GIT system. The SI has been revised, as reflected in ***Fig. R11*** (**new Supplementary *Figs. 2-4***). We believe that these revisions contribute to improving the overall clarity and readability of the manuscript.

Here, the new statement at the first paragraph of the Results and Discussion section: "Here, we report a gel-multiphasic ion transporter (GIT) that employs a unique cascade-heterointerface-trap to achieve soft-matter multistate ionic neuromorphics with ultralow energy consumption. We utilized a sequential phase-separated interface polymerization to fabricate the GIT materials. The GIT featured a triphasic separation system consisting of polyanion electrolyte disperse-phases (AEP) and polycationic electrolyte disperse-phases (CEP), interspersed within a low-conductive relay-medium phase (RMP), forming an integrated dual-cascaded heterointerface architecture (***Fig. 1a***). As shown in ***Supplementary Fig. 2***, through a sequential phase-separated interface polymerization process, 2-acrylanmido-2-methyl-1-propanesulfonic acid sodium (AMPAS) and (3-acrylanmidopyopyl) trimethyl ammonium chloride (ATAC) monomers formed the polyelectrolyte networks of the AEP and CEP, respectively, which exhibit opposite electrostatic properties. Within these phase-separated precursors, the compositional volume ratios between each polyelectrolyte dispersed phases and the RMP were kept constant, ensuring uniform phase separation and consistent sub-heterointerface density. Confocal laser scanning microscopy (CLSM) and scanning electron microscopy (SEM) confirmed the formation and structural integrity of the triphasic heterostructure, revealing AEP and CEP microinclusions with average diameters of approximately 2.5 μm uniformly dispersed within the continuous RMP matrix (***Supplementary Figs. 3a-3c***). Owing to the fixed molar ratio of polyelectrolyte networks between the AEP and CEP, solid-state zeta potential measurements demonstrated a stable electrostatic polarity contrast between the AEP and CEP sub-heterointerfaces (***Supplementary Fig. 3d***). The GIT materials with cascaded heterointerface architecture exhibited sustained mechanical robustness with an elastic modulus of approximately 0.6 MPa, and intrinsic environmental resistance (***Supplementary Fig. 4***). Within the heterointerface structures, the oleophilic RMP serves as a physical barrier that constrains swelling and dehydration of the polyelectrolyte disperse-phases, thereby enabling reliable ion transmission of the GIT systems under long-term aqueous and air conditions."

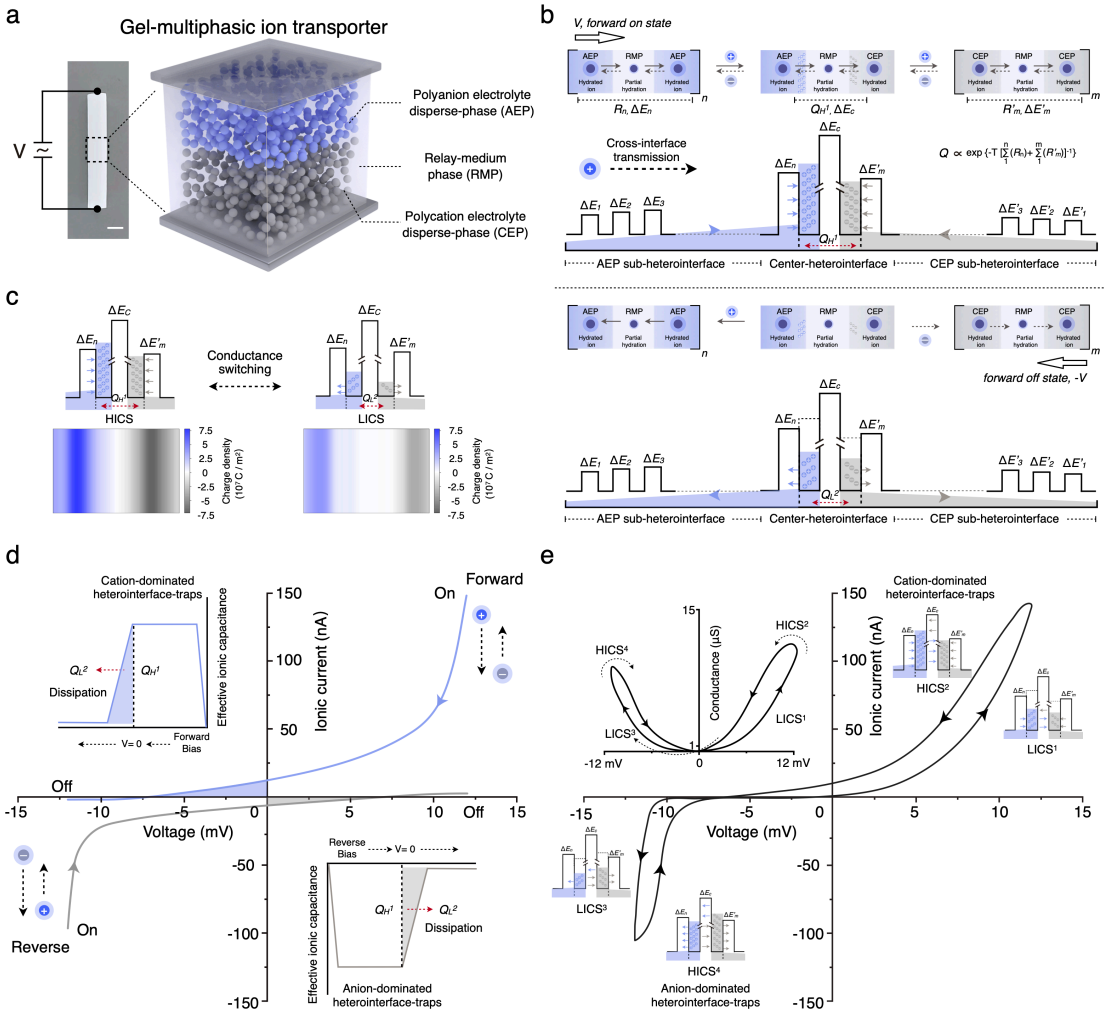

Fig. R10 ***(new Fig. 1) Cascade-heterointerface-trap ion transmission in gel-multiphasic ion transporters. a,*** *Structural illustration of the gel-multiphasic ion transporter (GIT), composed of an ion-enriched polyanion electrolyte disperse-phase (AEP), a relay medium-phase (RMP), and a polycation electrolyte disperse-phase (CEP). The triphase system integrates dual-cascaded-heterointerfaces: AEP sub-heterointerfaces, the center-heterointerface between AEP, RMP, and CEP, and CEP sub-heterointerfaces.* ***b,*** *Cascade-heterointerface-trap cation transmission mechanism. The heterointerfaces establish ionic cross-interface energy barrier gradients and cascading interionic interface retardation, driving cascade-heterointerfacial ion-traps featured by a weighting mechanism. ΔE_n ($\Delta E'_m$) and ΔEC represent cationic cross-interface transfer energy barriers at the sub-heterointerfaces and the center-heterointerface. Under alternating electric fields, the construction and dissipation of the center-heterointerface-trap as the pivotal ion-trap correspond to the high (HICS) and low (LICS) ion conductance states of GITs. Q represents generated effective ionic capacitance between*

cations and anions. ***c,*** *Molecular dynamics simulations demonstrate asymmetric accumulation and dissipation between cations and anions within the center-heterointerface-trap.* ***d,*** *Ionic bipolarity rectification of the* GIT_{Na} *under an alternating electric field ranging from 12 mV to -12 mV. Switching from HICS to LICS (i.e., on-to-off) in both arbitrary directions, respectively, corresponds to heterointerface-traps' construction and dissipation processes.* ***e,*** *Ionic neuromorphic effects of the* GIT_{Na} *under a periodic voltage sweep, where the ionic current-voltage (I-V) curve crosses at a non-origin point, and the ionic conductance-voltage (G-V) curve exhibits a crossing point at a negative voltage.*

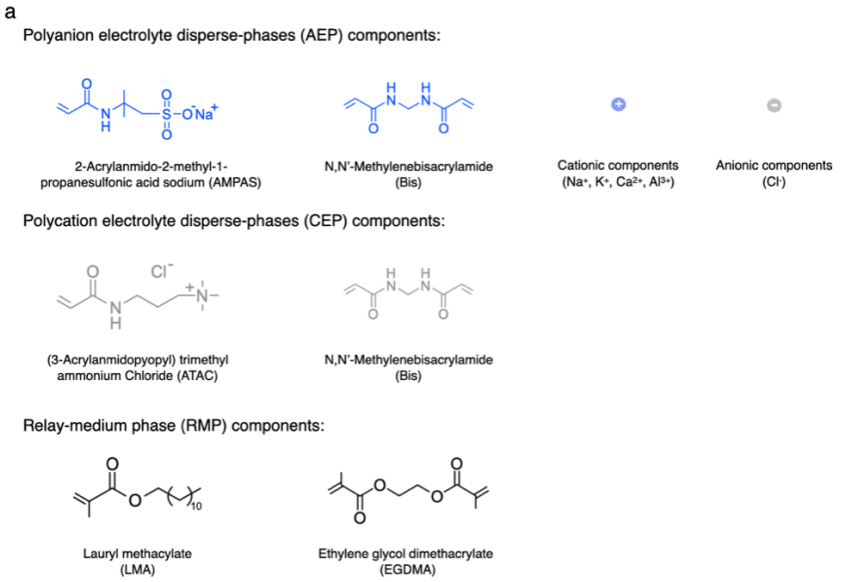

Supplementary Fig 2. Chemical structures of the GIT components.

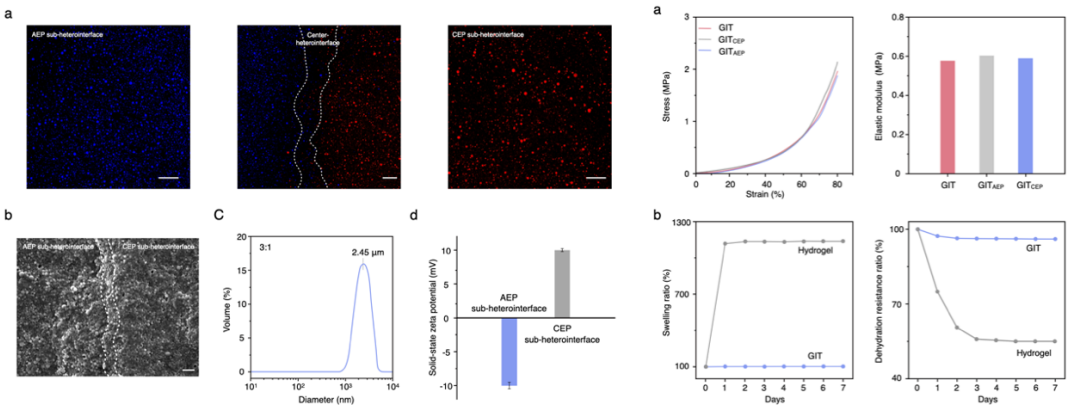

Supplementary Fig 3. Triphasic heterostructure characterization.

Supplementary Fig 4. Mechanical and environmental stability of GIT.

Fig. R11 ***(new Supplementary Figs. 2-4)*** *The material compositions and structural, mechanical characterizations, and environmental of the GIT system.*

Comment 1-2: *I would remove the long paragraph in Section 'Cascade-heterointerface-trap ion transmission', starting from 'The heterointerface architectures established ionic cross-interface transfer energy barriers (ΔE)…' to the end of the paragraph. The content here serves as an introduction, but it largely overlaps with the information in the abstract without giving any new information. Further, the many compound words/terms are difficult to read, failing to convey the meanings behind.*

Response: We sincerely appreciate the reviewer's constructive feedback regarding the clarity and conciseness of our manuscript. Following this comment, we have removed the first paragraph in the "Cascade-heterointerface-trap ion transmission" section and revised the section to focus on the material preparation and structural characterization of the GIT system. Please also refer to our response to **comment 1-1**. Furthermore, we have included a terminology index table in the revised SI to provide clear definitions for all key technical terms.

Comment 1-3: *The awkward terms include 'ionic cross-interface transfer energy barriers', 'cascade-heterointerface-traps governed ionic nonlinear transmission', 'asymmetric central interfacial charge accumulation', 'spike-strength/timing dependent dual-order (i.e., unipolar and bipolar) plasticity features', etc.*

Response: We apologize for the complexity of the terminology used in our original manuscript. While these specialized terms are essential to accurately describe the unique physical mechanisms of our GIT system, we recognize that their definitions must be more accessible. To address this, we have added a comprehensive terminology reference table (***Table R1***) to the revised SI. This table provides explicit physical definitions of the terms highlighted by the reviewer, as well as additional rectification and neuromorphic terminology, to facilitate a deeper understanding of our manuscript. Point-by-point clarification for the reviewer's specific mentions:

1. Ionic cross-interface transfer energy barriers (ΔE): The related energy consumption of ion cross-interface transport from the polyelectrolyte disperse-phase to the low-conductive relay-medium phase to the next polyelectrolyte disperse-phase.

2. Ionic nonlinear transmission: Under the applied electric field, the current-voltage relationship of ion transport no longer follows simple Ohm's law (i.e., a linear relationship) but instead exhibits a nonlinear response, representing a non-Ohmic phenomenon.

3. Asymmetric central interfacial charge accumulation: Owing to the distinct transmission efficiencies between cations and anions across cascaded sub-heterointerfaces, coupled with electrostatic partition

inversion at the center-heterointerface, both cations and anions undergo interface retardation effect at the center-heterointerface, leading to asymmetric charge accumulation.

4. Ionic bipolarity rectification: Compared to the unipolarity rectification with the fixed unidirectional conduction transition (i.e., on-to-off, forward electrical field; off-to-on, reverse electrical field), the bipolarity rectification represents a bipolar conduction transition from high to low conductance under both directional electrical field (i.e., on-to-off, forward and reverse electrical field).

5. Spike-strength/timing dependent plasticity: The postsynaptic current responds dynamically according to the amplitude and relative timing of spikes.

6. Dual-order (i.e., unipolar and bipolar) plasticity: Dual-order plasticity denotes the distinct conductance modulation process in the GIT system for different *I-V* hysteresis behaviors, where the system exhibits either dual-set transitions (unipolar) or set/reset transitions (bipolar). Under periodic *I-V* scanning, unipolar plasticity represents an identical conductance transition trend across different *I-V* quadrants (e.g., LICS to HICS (set)). Bipolar plasticity represents opposite conductance transition trends across different *I-V* quadrants (e.g., LICS to HICS (set) and HICS to LICS (reset)).

Table R1 ***(Supplementary Table 4)*** *Corresponding explanation of the professional terminologies used in this work.*

Professional terminologies	Corresponding explanation
Ionic cross-interface transfer energy barriers	The related energy consumption of ion cross-interface transport from the polyelectrolyte disperse-phase to the low-conductive relay-medium phase to the next polyelectrolyte disperse-phase.
ionic nonlinear transmission	Under the applied electric field, the current-voltage relationship of ion transport no longer follows simple Ohm's law (i.e., a linear relationship) but instead exhibits a nonlinear response, representing a non-Ohmic phenomenon.
Asymmetric central interfacial charge accumulation	Owing to the distinct transmission efficiencies between cations and anions across cascaded sub-heterointerfaces, coupled with electrostatic partition inversion at the center-heterointerface, both cations and anions undergo interface retardation effect at the center-heterointerface, leading to asymmetric charge accumulation.
Ionic bipolarity rectification	Compared to the unipolarity rectification with the fixed unidirectional conduction transition (i.e., on-to-off, forward electrical field; off-to-on, reverse electrical field), the bipolarity rectification represents a bipolar conduction transition from high to low conductance under both directional electrical field (i.e., on-to-off, forward and reverse electrical field).
Spike-strength/timing dependent plasticity	The postsynaptic current responds dynamically strengthened or weakened (modulated) according to the amplitude and relative timing of spikes.
Dual-order (i.e., unipolar and bipolar) plasticity	Dual-order plasticity denotes the distinct conductance modulation process in the GIT system for different *I-V* hysteresis behaviors, where the system exhibits either dual-set transitions (unipolar) or set/reset transitions (bipolar). Under periodic *I-V* scanning, unipolar plasticity represents an identical conductance transition trend across different *I-V* quadrants (e.g., LICS to HICS (set)). Bipolar plasticity represents opposite conductance transition trends across different *I-V* quadrants (e.g., LICS to HICS (set) and HICS to LICS (reset)).
Short-term (ST) and long-term (LT) behaviors	The retention time of the postsynaptic current, which corresponds to the decay time of the peak postsynaptic current to its baseline after paired stimulation, with ST defined as ≤ 1 s and LT as > 1 s.
Postsynaptic ionic current change (Δi)	$\Delta i = i_2 - i_1$, where i_1 and i_2 represent the postsynaptic ionic currents generated by the first and second voltage pulses, respectively.
Paired-pulse facilitation/depression retention times ($t_{r,PPF}$ and $t_{r,PPD}$)	The retention time of the facilitation or depression-type postsynaptic current after paired stimulation.
Plasticity factor (k)	The slope of t_r with respect to the amplitude of the spike voltage.
Synaptic connection strength (ΔG)	$\Delta G = (G_F - G_O)/ G_O$, where G_O and G_F represent the conductance values measured under the original and final spikes.

Comment 1-4: *I strongly recommend replotting Fig. 1b to 1e to first divide the CV scan into multiple steps/regions and correlate the mechanistic schematics (1b) aside to give explanations. The same for Fig. 3a to c.*

Response: We thank the reviewer for this valuable suggestion to enhance the clarity of our mechanistic explanations. We have revised the details of ***Fig. R10*** ***(new Fig. 1)*** and ***Fig. R12*** ***(new Figs. 3a-3c)*** to highlight the dynamic heterointerface-trap states and their correspondence under different electric-field scanning conditions. ***Figs. 1b-d*** illustrate ionic bipolarity rectification modulated by the cascade-heterointerface-trap mechanism in the GIT system. Under a forward electric field, the system first reaches a high ion conductivity state (HICS), corresponding to the effective ionic capacitance Q_H^1. Subsequently, under a reverse electric field, ion dissipation within the center-heterointerface-trap drives the GIT system into the low ion conductivity state (LICS), corresponding to the effective ionic capacitance Q_L^2. Accordingly, we have comprehensively revised the details of effective ionic capacitance in ***Figs. 1b-1d*** to explicitly reflect the two conductance states under polarity switching. In addition, ***Fig. 1e*** and ***Figs. 3a-3c*** present the dual-order memristive behavior of the GIT material with cascade-heterointerface-trap dynamics. Specifically, ***Fig. 1e*** shows the *I-V* hysteresis loops under periodic electric-field scanning, with the inset highlighting the dynamic transition of conductance. All relevant details have been relabeled according to the sequence of conductance states formed by the applied electric fields, and corresponding schematics are provided for each scanning quadrant. Following the reviewer's suggestion, we have further revised the details in ***Figs. 3a-3c*** to establish a correspondence between the *I-V* hysteresis loops and the schematic of heterointerface-trap dynamics. In unipolar plasticity, the dual-set features correspond to the transition from LICS to HICS, and we also provide the corresponding schematics illustrating accumulation and dissipation in heterointerface-trap dynamics. In bipolar plasticity, the GIT system exhibits opposite conductance transitions across different *I-V* scanning quadrants, including LICS-to-HICS (set) and HICS-to-LICS (reset), accompanied by corresponding schematics illustrating saturation accumulation, dissipation, and depletion in heterointerface-trap dynamics. These newly added schematics correspond to the original Roman numeral labels used during the dual-order scanning process. Overall, the revised illustrations now provide a clearly segmented analysis of the *I-V* cure and hysteresis loops, accompanied by directly aligned schematics of the mechanisms.

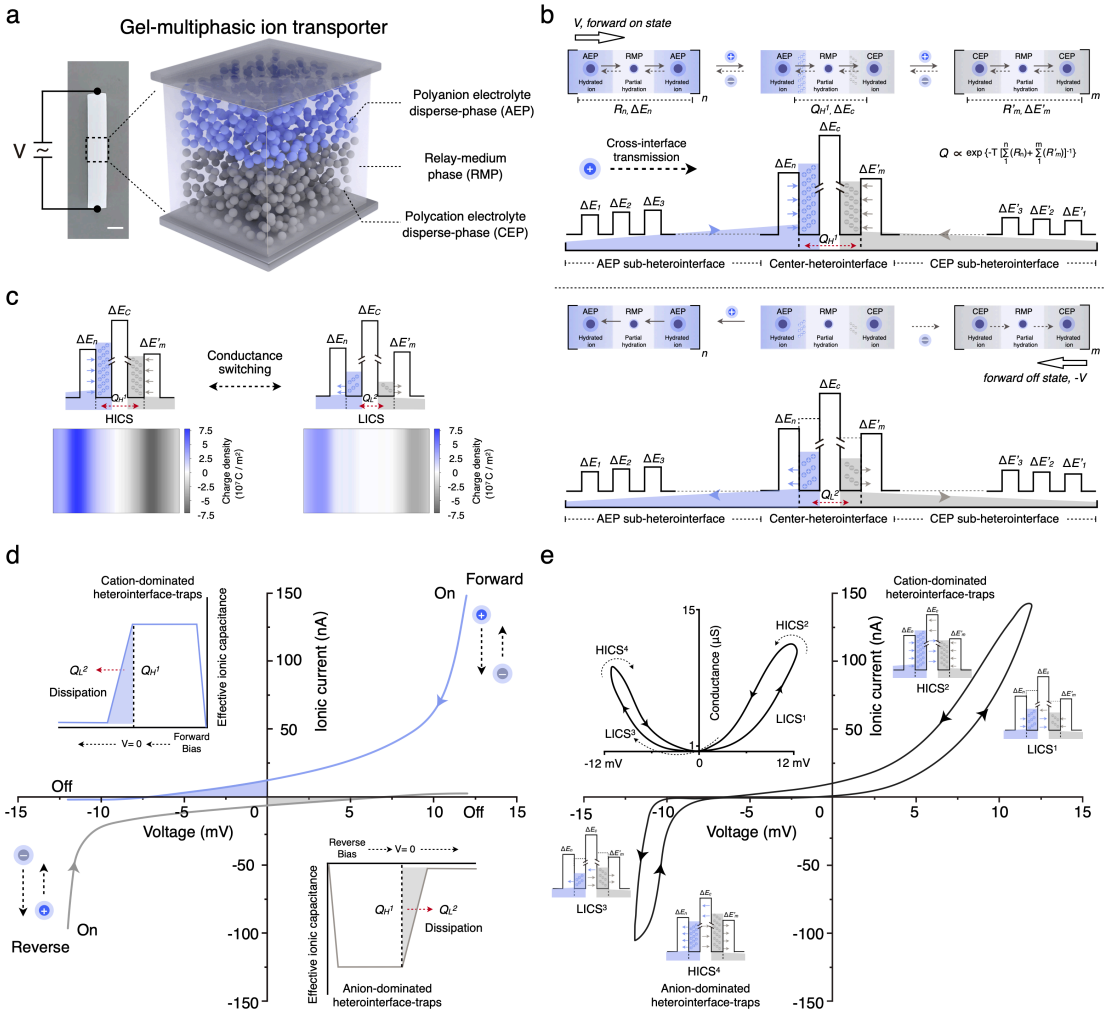

***Fig. R10* (new Fig. 1) Cascade-heterointerface-trap ion transmission in gel-multiphasic ion transporters. a,** *Structural illustration of the gel-multiphasic ion transporter (GIT), composed of an ion-enriched polyanion electrolyte disperse-phase (AEP), a relay medium-phase (RMP), and a polycation electrolyte disperse-phase (CEP). The triphase system integrates dual-cascaded-heterointerfaces: AEP sub-heterointerfaces, the center-heterointerface between AEP, RMP, and CEP, and CEP sub-heterointerfaces.* **b,** *Cascade-heterointerface-trap cation transmission mechanism. The heterointerfaces establish ionic cross-interface energy barrier gradients and cascading interionic interface retardation, driving cascade-heterointerfacial ion-traps featured by a weighting mechanism. ΔE_n ($\Delta E'_m$) and ΔEC represent cationic cross-interface transfer energy barriers at the sub-heterointerfaces and the center-heterointerface. Under alternating electric fields, the construction and dissipation of the center-heterointerface-trap as the pivotal ion-trap correspond to the high (HICS) and low (LICS) ion conductance states of GITs. Q represents generated effective ionic capacitance between*

cations and anions. ***c,*** *Molecular dynamics simulations demonstrate asymmetric accumulation and dissipation between cations and anions within the center-heterointerface-trap.* ***d,*** *Ionic bipolarity rectification of the* GIT_{Na} *under an alternating electric field ranging from 12 mV to -12 mV. Switching from HICS to LICS (i.e., on-to-off) in both arbitrary directions, respectively, corresponds to heterointerface-traps' construction and dissipation processes.* ***e,*** *Ionic neuromorphic effects of the* GIT_{Na} *under a periodic voltage sweep, where the ionic current-voltage (I-V) curve crosses at a non-origin point, and the ionic conductance-voltage (G-V) curve exhibits a crossing point at a negative voltage.*

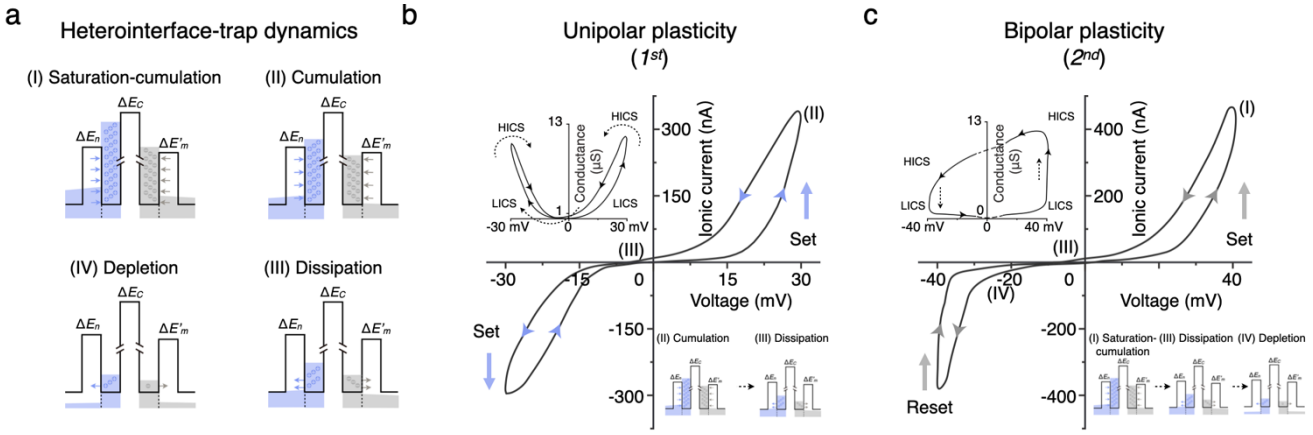

Fig. R12 ***(new Figs. 3a-3c)*** *(a) Schematic illustration of heterointerface-trap dynamics. Saturation-cumulation (I) and cumulation (II) describe the degree of ion accumulation within the center-heterointerface-trap, corresponding to different electric field strengths. Dissipation (III) and depletion (IV) describe the effusion processes of trapped ions, diminishing effective ionic capacitance under reverse electric fields. (b and c) Distinct I-V and G-V characteristic curves of the* $GIT_{Ca/Al}$ *exhibit dual-order (i.e., unipolar and bipolar) plasticity transitions through modulation of periodic electric field strengths. Both I-V curves intersect at a non-origin point. In the unipolar state (*1^{st}*), the G-V curve shows a crossing point at a negative voltage, while in the bipolar state (*2^{nd}*), it exhibits a simple open-loop pattern.*

Comment 1-5: *Many terms used in this manuscript are also misleading. 'bidirectional ionic rectification' does not make sense to me. Rectification in the context of iontronics means that only one direction of ionic current can pass, i.e., it behaves as a diode. The 'bidirectional' nullifies this term. Also, the same effect has been widely observed in biological nanopores and correlated dropletronic memristive devices (DOI: 10.1039/d5cs00580a). The authors should mention this and provide a*

discussion.

Response: We deeply appreciate the reviewer for raising the important concern regarding the terminology of ionic bipolarity rectification. We would further like to emphasize that the bipolarity rectification represents a bipolar conduction transition from high to low conductance under both directional electrical field (i.e., on-to-off, forward and reverse electrical field), compared to the unipolarity rectification with a unidirectional conduction transition (i.e., on-to-off, forward electrical field; off-to-on, reverse electrical field). This bipolarity rectification behavior differs from previous unidirectional rectification with unipolar characteristics. However, to avoid potential misunderstandings, we have replaced the term with "ionic bipolarity rectification" in the revised manuscript.

We would further like to clarify that the bipolar conductance behavior of the GIT system has been systematically demonstrated in ***Figs. 2a-2c***. As shown in ***Fig. 2f*** and ***Supplementary Table 2***, we provide a detailed comparative analysis between our GIT system and other ionic rectification systems, including artificial nanopore and nanofluidic ionitroincs. Existing ionic rectifiers, including traditional nanofluidic and polyelectrolyte-based diodes, typically exhibit unipolarity rectification with unidirectional constrained by static structural asymmetries and fixed polarity, and often rely on relatively high alternating electric fields. We also conduct a comprehensive analysis of bilayer hydrogel systems with the same chemical structures and compositions (***Fig. 2e***). These systems, governed by electric double-layer effects, demonstrate unidirectional ionic rectification, further highlighting the unique nature of the ionic bipolarity rectification achieved in our GIT system. According to the reviewer's suggestion, we will further cite this article (*Chem. Soc. Rev.* **55**, 299-335 (2026)). Regarding biological nanopores (biological ion channels), we fully agree with the reviewer's view that they typically exhibit unidirectional ionic transport. At the level of biological cell membranes and synaptic interfaces, researchers have also found that signal transmission is inherently bidirectional and supports similar rectification behaviors, including inward and outward rectification (*Nat. Commun.* **9**, 1096 (2018), *Nat. Chem. Biol.* **10**, 188-195 (2014), and *Nat. Neurosci.* **8**, 279-287 (2005)). As reflected in ***Supplementary Fig. 1***, we also emphasize this point in our manuscript. We further thank the reviewer for this important comment, which helps us clarify the distinct ionic bipolarity rectification characteristics observed in the GIT system.

Comment 1-6: *The term 'neuromorphic' has also been widely used in this manuscript. However, its meaning is imprecise. 'Memristive' is a better and more accepted replacement.*

Response: We appreciate the reviewer's suggestion to use "memristive". In the specific field of ionic neuromorphics, the term "memristive" inherently encompasses both plasticity and memory behaviors. For this reason, the term "memristive" has been frequently used to reflect the dual-order plasticity, short- and long-term memory effects, and spike-strength/timing dependent plasticity demonstrated in our system (***Fig. 3***). Following the reviewer's suggestion, we will further emphasize the term "memristive" in this section, such as "plasticity and memristive effects".

We would like to emphasize that the definition of "neuromorphic" should encompass a broader scope. As highlighted in the referenced literature, "neuromorphic processing and sensing" has been recognized as a key functional in bioelectronics, particularly in the context of responding and processing input upstream signals (*Chem. Rev.* **125**, 2625-2664 (2025)). In addition, related concepts such as neuromorphic skin and neuromorphic bioelectronics have also been extensively discussed in these studies (*Nat. Electron.* **7**, 525-536 (2024), *Nat. Rev. Mater.* **9**, 134-149 (2024)). In our work, "neuromorphic" describes the combined features of ionic bipolarity rectification, multistate plasticity and memristive effects, and neural signal processing capability. We also demonstrate distinct learning behaviors (Hebbian, anti-Hebbian, and Bienenstock-Cooper-Munro learning rule) capabilities that differ from other memristors, which are an important manifestation of neuromorphics. Importantly, we developed a biohybrid neural circuit by interfacing a GIT-based neuro-iontronic processor with the rat's transected sciatic nerve, realizing bioneuron-driven ionic neuromorphic processing for interneural signal reconfiguration and plasticity modulation.

Comment 1-7: *The paragraph that starts with 'As illustrated in Fig. 1b and Supplementary Fig. 2…' is essential but difficult to read. I strongly recommend a rewrite with clear words and shorter sentences.*

Response: We thank the reviewer for this helpful suggestion. We have revised this paragraph by simplifying the wording and breaking the original long sentences into shorter statements. The revisions are as follows: "The heterointerface architectures established ionic cross-interface transfer energy barriers (ΔE) accompanied by hydration-to-partial-dehydration alternating transitions. Meanwhile, the combination of heterointerfacial electrostatics and steric hindrance induced a spatially graded ΔE landscape, leading to interionic retardation across cascaded interfaces and ultimately the formation of heterointerface-traps. The cascade-heterointerface-trap modulated the cation and anion cross-interface

transmission, which corresponded to the conductance state of the GIT under alternating electric fields (***Fig. 1b and Supplementary Fig. 5***). Initially, the AEP acted as an ion-enriched phase, containing both fixed polyelectrolyte counter-cations and mobile electrolyte cations and anions, while the CEP contained mobile polyelectrolyte counter-anions. Under a forward electric field, hydrated cations were driven from the AEP sub-heterointerface side and had to overcome both the AEP electrostatic attractions and the RMP spatial repulsive interactions. Due to the electrostatic interactions and spatial steric hindrance at heterointerfaces, cations experienced a graded sequence of cross-interface ΔE, triggering a gradient of interionic interface retardation. At the CEP sub-heterointerfaces, the transport of free hydrated anions also experienced graded cross-interface energy barriers, analogous to those encountered by cations on the opposite side. Originating from the electrostatic partitioning established at the dual polyelectrolyte heterointerfaces, cations and anions migrated respectively toward the center-heterointerface, which featured the reversal of electrostatic interactions. This region exhibited the most pronounced ΔE_C and interionic retardation effects, forming the pivotal heterointerface-trap within GIT systems (***Supplementary Fig. 6***). Owing to the distinct quantities and transmission efficiencies between cations and anions across cascaded sub-heterointerfaces, the center-heterointerface-trap region possessed an asymmetrical distribution of cationic and anionic accumulation. In GIT systems, the effective ionic capacitance (Q) within the center-heterointerface-trap functioned as a charge reservoir. Dynamically, the formation of cation-dominated heterointerface-traps induced the emergence of a built-in positive ionic potential field, aligning with the applied electric field. This further enhanced cross-interface migration and convergence of cations and anions. Thus, a high ion conductance state (HICS) of the GIT system was constructed. Through an equivalent capacitance-resistance model, the Q reflects the heterointerface-trap strength, as described by $Q \propto \exp\{-T[\sum_1^n(R_n) + \sum_1^m(R'_m)]^{-1}\}$. The R_n and R'_m represent the resistance of the AEP and CEP sub-heterointerfaces, respectively. Subsequently, a reverse electric field prompted the effusion of cations and anions from the central heterointerface toward both sub-heterointerfaces, dissipating the localized ionic reservoir and transitioning the system into a low ion conductance state (LICS). As shown in ***Fig. 1c and Supplementary Fig. 8***, MD simulations confirmed the asymmetric accumulation and dissipation of ions within the central heterointerface, demonstrating that the dynamics of the cation-dominated heterointerface-trap correlated with the system's conduction switching behavior. This model also captured the strength of heterointerface-traps as a dynamic function of the applied electric field over time. Experimentally, the relaxation-time energy spectrum displayed the interfacial ionic potential

evolution and distribution behaviors in the center-heterointerface related region under a dynamically applied electric field (***Supplementary Fig. 9***). Upon field application, asymmetric cationic and anionic potentials progressively developed within the heterointerface region, exhibiting interfacial ionic accumulation and the formation of the heterointerface-trap. When the bias returned to zero and the field was removed, the accumulated heterointerface-trap could not be sustained, resulting in rapid ionic dissipation. This observed process was indicative of hysteretic ionic relaxation dynamics governed by the construction and dissipation of the heterointerface-traps."

Comment 2-1: *My understanding of the GIT is that it comprises two oppositely charged HBGs and forms an iontronic diode structure. In addition to conventional iontronic diodes, the unique structure of the HBGs induces a significant capacitance effect at the center heterointerface, so-called the relay medium phase (RMP), which results in the memristive feature.*

I don't understand why $\Delta E_n > \ldots > \Delta E_2 > \Delta E_1$. *The HBG is evenly distributed, and the cross-interface transfer energy barriers should be the same. Of course, their accumulation cascades, e.g., the working mechanism of HBG.*

Response: We thank the reviewer for this insightful comment and the opportunity to clarify the distinction between our previous work and the present study. In previous work, the study primarily focuses on ion differentiated cross-heterointerface transport, where the transport behavior is governed by heterogated-dominated transfer energy barriers (ΔE). At the single heterointerface scale, the previous work primarily emphasizes the mechanism of ion cross-interface transmission, which is closely associated with ionic hydration and dehydration energetics. Molecular dynamics simulations are also employed to quantitatively resolve the transfer free energy barriers of different ions crossing the single heterointerface. At the material scale, an equivalent resistance model is used to demonstrate the transmission behavior of different ions across cascaded-heterointerfaces. Accordingly, the previous work does not consider interionic interactions during the transport process or discuss whether multiple heterointerfaces possess identical or non-identical transfer energy barriers.

In contrast, the present study incorporates both interionic interactions and ion-electrostatic coupling during transport across multiple cascaded-heterointerfaces. In the process of realistic ion cross-interface transmission, the dynamics cross-interfacial ΔE inevitably exists, arises from the synergistic effect of heterointerfacial electrostatics, steric confinement, and interionic interactions at the polyelectrolyte-RMP boundaries. Molecular dynamics (MD) simulations further confirm this point

(***Supplementary Fig. 7***). As noted in our manuscript, during ion cross-interface transmission process, the retardation of ionic cross-interface transport, coupled with electrostatic polarization, dynamically induces the ΔE gradient landscape, establishing each heterointerface as an effective kinetic trap. As illustrated in ***Fig. 1b*** and ***Supplementary Fig. 5***, under a forward electric field, cations and anions undergo stepwise interfacial retardation accumulation at successive sub-heterointerfaces, thereby producing a gradient of ΔE_n and retardation along the transport direction. Concurrently, the ions migrate respectively toward the center-heterointerface, which feature the reversal of electrostatic interactions, this region exhibits the most pronounced ΔE_C and interionic retardation effects, forming the pivotal heterointerface-trap within GIT systems. Compared with our previous work on ion-selective transport, the resulted cascaded-heterointerface-trap dynamics enable the GIT system to realize ionic bipolarity rectification and multistate ionic memristive functionalities, including distinctive ionic bipolarity rectification (on/off ratio>10^3), voltage-event dual-order (unipolar and bipolar) plasticity, short- and long-term memory, and ion-based BCM and Hebbian learning rules.

Comment 2-2: *'Initially, AEP acted as a cation- and anion-enriched phase, while CEP contained free anions.' What do you mean? Shouldn't AEP only contain free cations?*

Response: We sincerely thank the reviewer for this insightful comment, which has helped us clarify the description of our materials. As described in the SI, the polyanion electrolyte heterogel precursor contains polymerizable polyanion electrolyte monomers together with a preloaded electrolyte solution. Therefore, the AEP includes mobile polyelectrolyte counter-cations as well as freely mobile electrolyte cations and anions originating from the preloaded electrolyte. In contrast, the CEP contains mobile polyelectrolyte counter-anions. To avoid any further ambiguity, the manuscript text have been revised as follows: "Initially, the AEP acted as an ion-enriched phase, containing both fixed polyelectrolyte counter-cations and mobile electrolyte cations and anions, while the CEP contained mobile polyelectrolyte counter-anions."

Comment 2-3: *The calculation of forward (f) and reverse (f') rectification ratios is unclear. The methods used in conventional iontronic diodes should be considered, and the performance under alternating voltages should be measured.*

Response: We fully agree with the reviewer. In our work, the forward (f) and reverse (f') rectification ratios were calculated following the conventional definitions widely used in iontronic and nanofluidic

diode studies. Owing to the reverse current carries a negative sign, the absolute value of current magnitudes is used in the rectification ratio calculation. While the negative sign in the *f'* formula is used specifically to denote the opposite polarity relative to the forward rectification, ensuring a clear distinction between the two states. To avoid ambiguity, we have now explicitly clarified the calculation method in the SI. The relevant content is as follows: "The forward rectification ratio (*f*) was calculated as $f = |+i_{max}/-i_{max}|$ and the reverse rectification ratio (*f'*) was calculated as $f' = -|-i_{max}/+i_{max}|$."

Comment 2-4: *The influence of frequency and scanning rates should be further explained in the rectification section and clearly shown in the Figures.*

Response: We appreciate the reviewer for raising this important point. Following the reviewer's suggestion, we have supplemented the rectification section with systematic analyses of both scanning-rate-dependent and frequency-dependent rectification behaviors, and the corresponding results have been clearly presented in the revised manuscript and SI. As shown in ***Fig. R13***, we systematically investigate the rectification behavior of the GIT_{Na} system over a scanning-rate range from 0.1 to 10 mV/s by analyzing the corresponding *I-V* characteristics under alternating electric fields. The results reveal that the rectification performance exhibits a clear inverse dependence on the scanning rate. At a slower scanning rate (0.1 mV/s), sufficient time is provided within each voltage sweep for ionic accumulation in the cascade-heterointerface-trap, leading to pronounced rectification. In contrast, at a faster scanning rate (10 mV/s), the shortened sweep time limits the establishment of ionic accumulation within the cascade-heterointerface-trap, resulting in weakened rectification. Furthermore, we investigate the frequency correlation of ionic bipolarity rectification by varying the time intervals (from 0.1 s to 1 s) between successive scanning cycles while maintaining a fixed scan rate at 1 mV/s (***Fig. R14***). Our results demonstrate that the bipolarity rectification ratio remains remarkably stable across a range of intervals, consistently maintaining its magnitude within the same order of magnitude. This stability arises from the intrinsic nature of the bipolarity rectification cycle, in which the reverse scanning process effectively resets the ion transport state of the cascaded-heterointerface-traps, thereby initializing the ion transmission for the subsequent rectification cycle. As a result, the rectification behavior is insensitive to variations in the time interval within this range. We appreciate the reviewer's constructive comment. The corresponding results have been added to the revised ***Supplementary Fig. 15***, and discussion have been included in revised manuscript.

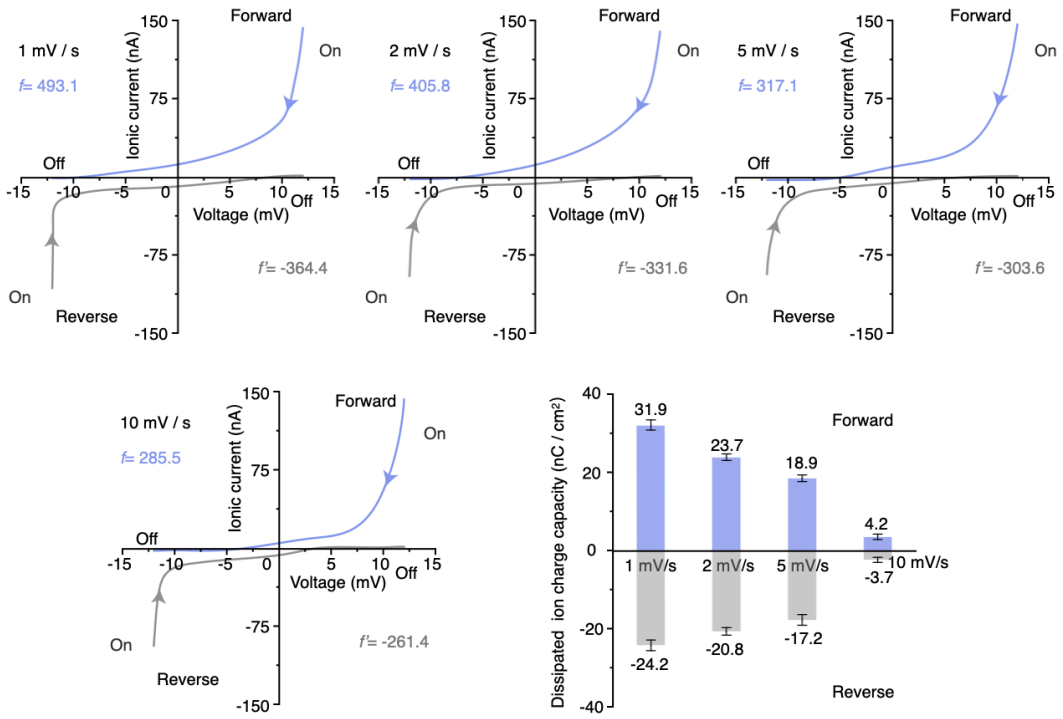

Fig. R13 *Bipolarity asymmetric I-V curves of the GIT_{Na} under varying voltage scan rates (1 mV/s, 2 mV/s, 5 mV/s, and 10 mV/s), and related dissipated ion charge capacities.*

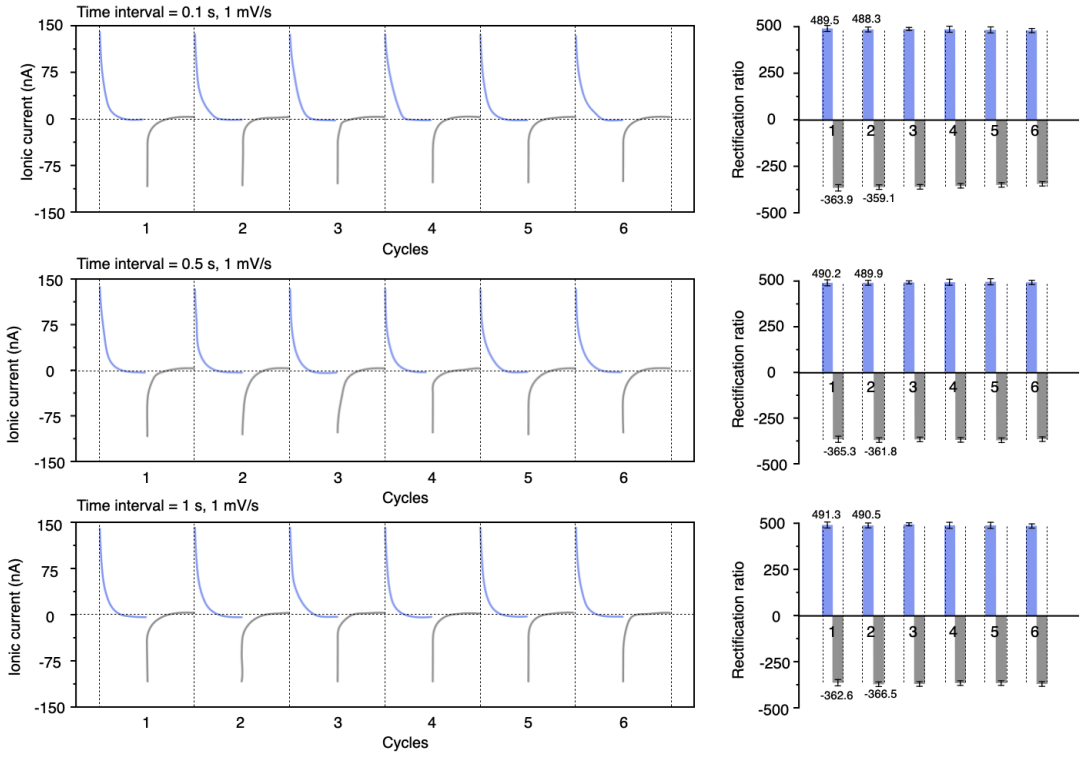

Fig. R14 ***(new Supplementary Fig. 15b)*** *Bipolarity rectification cycles of the GIT_{Na} under varying time intervals (0.1 s, 0.5 s, and 1 s).*

Comment 2-5: *The part 'The GIT material was fabricated through a…' should be moved to the beginning.*

Response: We appreciate the reviewer for this helpful suggestion. Following the reviewer's recommendation, we have moved the description beginning. And the revised text is as follows: "Here, we report a gel-multiphasic ion transporter (GIT) that employs a unique cascade-heterointerface-trap to achieve soft-matter multistate ionic neuromorphics with ultralow energy consumption. We utilized a sequential phase-separated interface polymerization to fabricate the GIT materials. The GIT featured a triphasic separation system consisting of polyanion electrolyte disperse-phases (AEP) and polycationic electrolyte disperse-phases (CEP), interspersed within a low-conductive relay-medium phase (RMP), forming an integrated dual-cascaded heterointerface architecture (***Fig. 1a***). As shown in ***Supplementary Fig. 2***, through a sequential phase-separated interface polymerization process, 2-acrylanmido-2-methyl-1-propanesulfonic acid sodium (AMPAS) and (3-acrylanmidopyopyl) trimethyl ammonium chloride (ATAC) monomers formed the polyelectrolyte networks of the AEP and CEP, respectively, which exhibit opposite electrostatic properties. Within these phase-separated precursors, the compositional volume ratios between each polyelectrolyte dispersed phases and the RMP were kept constant, ensuring uniform phase separation and consistent sub-heterointerface density. Confocal laser scanning microscopy (CLSM) and scanning electron microscopy (SEM) confirmed the formation and structural integrity of the triphasic heterostructure, revealing AEP and CEP microinclusions with average diameters of approximately 2.5 μm uniformly dispersed within the continuous RMP matrix (***Supplementary Figs. 3a-3c***). Owing to the fixed molar ratio of polyelectrolyte networks between the AEP and CEP, solid-state zeta potential measurements demonstrated a stable electrostatic polarity contrast between the AEP and CEP sub-heterointerfaces (***Supplementary Fig. 3d***). The GIT materials with cascaded heterointerface architecture exhibited sustained mechanical robustness with an elastic modulus of approximately 0.6 MPa, and intrinsic environmental resistance (***Supplementary Fig. 4***). Within the heterointerface structures, the oleophilic RMP serves as a physical barrier that constrains swelling and dehydration of the polyelectrolyte disperse-phases, thereby enabling reliable ion transmission of the GIT systems under long-term aqueous and air conditions.

The heterointerface architectures established ionic cross-interface transfer energy barriers (ΔE) accompanied by hydration-to-partial-dehydration alternating transitions. Meanwhile, the combination of heterointerfacial electrostatics and steric hindrance induced a spatially graded ΔE landscape, leading to interionic retardation across cascaded interfaces and ultimately the formation of heterointerface-traps.

The cascade-heterointerface-trap modulated the cation and anion cross-interface transmission, which corresponded to the conductance state of the GIT under alternating electric fields (***Fig. 1b and Supplementary Fig. 5***). Initially, the AEP acted as an ion-enriched phase, containing both fixed polyelectrolyte counter-cations and mobile electrolyte cations and anions, while the CEP contained mobile polyelectrolyte counter-anions…."

Comment 2-6: *The influence of various ion species is important. Could the authors try protons?*

Response: We sincerely thank the reviewer for this constructive suggestion. Following the reviewer's recommendation, we have performed additional experiments of the GIT system with protons (H^+) and anions (Cl^-) as charge carriers. The new GIT material is prepared by introducing HCl as the electrolyte into the AEP, while all other fabrication conditions remain unchanged. As shown in ***Fig. R15***, the proton-transported GIT exhibits clear ionic bipolarity rectification, *I-V* hysteresis loop, and paired-pulse plasticity, indicating that the cascade-heterointerface-trap mechanism remains operative during this process. Under dynamic electric fields, the accumulation and dissipation of protons and anions within cascaded-heterointerface-traps dominate the observed ionic bipolarity rectification and memristive behaviors. Compared with GIT_{Na}, the GIT with proton transmission exhibits bigger rectification ratio and more pronounced postsynaptic spike current under the same testing conditions, owing to the intrinsically higher mobility of protons that enables more rapid ionic accumulation.

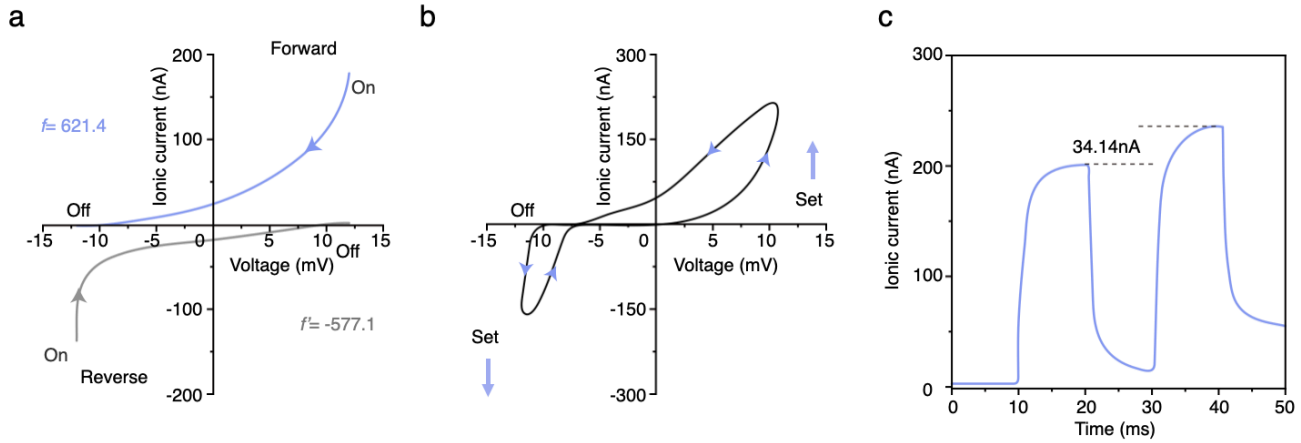

Fig. R15 *Ionic bipolarity rectification, I-V hysteresis loop, and paired-pulse measurements of the GIT with proton transmission.*

Comment 2-7: *The mechanism of ion concentration is unclear. The results in SI Fig. 16 seem to show that higher ion concentration shows higher ion rectification, which is contradictory to the explanation in the main text.*

Response: We thank the reviewer for identifying this inconsistency. We acknowledge that the original statement in the main text is incorrect and has now been revised. The revised text is as follows: "Meanwhile, as the NaCl concentration decreased from 1M to 0.1M within the AEP, the values of f and *f'* for the GIT_{Na} decreased to 194.9 and -126.9 (***Supplementary Fig. 16a***)."

Comment 2-8: *The hydrogel materials (bilayer polyelectrolyte hydrogel$_{Ca/Al}$) should be clearly explained. Different hydrogel materials may provide different performances.*

Response: We are grateful to the reviewer for this comment. In our manuscript, the comparison between bilayer polyelectrolyte hydrogels and GIT materials involves two points. First, we utilized the composition and structure of the GIT electrolyte phase to construct a typical bilayer hydrogel material. Structurally and mechanistically, this bilayer polyelectrolyte hydrogel is equivalent to the class of materials widely reported in the literature (*J. Am. Chem. Soc.* **129**, 10801-10806 (2007), *Nat. Commun.* **13**, 6669 (2022), and *Adv. Funct. Mater.* **33**, 2211316 (2023)), which primarily rely on electric double layer (EDL)-dominated interfacial polarization to induce unipolarity ionic rectification (***Supplementary Fig. 19***). Although the rectification behavior of such hydrogel systems can be modulated by varying hydrogel monomers or charge density, their transport mechanism remains governed by the EDL effect. Consequently, these systems typically exhibit limited rectification ratio, are restricted to unipolarity rectification, and are unable to support memristive behavior. And the absence of a self-crossing *I-V* loop in the bilayer polyelectrolyte hydrogel$_{Ca/Al}$ is also shown in ***Supplementary Fig. 26***. In addition, swelling tests reveal that the bilayer polyelectrolyte hydrogels do not maintain stable rectification behavior under aqueous conditions. Moreover, inevitable internal ion diffusion within the bilayer structures leads to a noticeable decay of rectification within 24 h. In stark contrast, the GIT system sustained *f* and *f'* exceeding 10^3 over multiple bipolarity rectification cycles, with no observable performance degradation (***Fig. 2e and Supplementary Fig. 20***). The cascade-heterointerface structure exhibited effective shielding capabilities against ion diffusion. In continuous operation tests, long-term rectified performance and stability are further confirmed by the asymmetric ionic signals observed in the GIT_{Na} and the $GIT_{Ca/Al}$ (***Supplementary Fig. 21***).

Furthermore, we systematically compare GIT materials with previously reported bilayer

polyelectrolyte hydrogel-based ion rectification materials possessing different chemical structures and compositions. As shown in ***Fig. 2f*** and ***Supplementary Table 2***, bilayer polyelectrolyte hydrogels governed by EDL polarization, despite variations in polymer backbone, charge density, and electrolyte composition, consistently exhibit unipolar rectification with limited rectification ratios. In addition, these systems require relatively high operating voltages and do not display memristive behavior. These results demonstrate that the observed transport behaviors are intrinsic to the EDL-dominated hydrogel mechanism rather than dependent on specific gel chemistries. In contrast, the GIT system, enabled by cascaded-heterointerface-trap architectures, exhibits unconventional ionic bipolarity rectification under ultralow voltage-driven fields, highlighting a fundamentally distinct transport mechanism beyond conventional gel-based rectifiers.

Comment 2-9: *I don't understand the need to differentiate the unipolar and bipolar plasticity features. Isn't the unipolar state a part of the bipolar state?*

Response: We appreciate the reviewer for this comment. At the experimental level, unipolar and bipolar plasticity are investigated using two distinct electrical testing protocols. Unipolar and bipolar plasticity are not defined as a subset relationship in the iontronic and memristive literature, but rather as two distinct operation modes characterized by different polarity requirements. Specifically, unipolar plasticity represents an identical conductance transition trend across different *I-V* quadrants (e.g., LICS to HICS (set)). Bipolar plasticity represents opposite conductance transition trends across different *I-V* quadrants (e.g., LICS to HICS (set) and HICS to LICS (reset)). In our study, unipolar and bipolar plasticity exhibit identical conductance switching behavior in the first *I-V* quadrant. However, they become clearly distinct in the fourth quadrant, where polarity-reversed conductance switching is observed exclusively in bipolar plasticity and is absent under unipolar operation. This experimental distinction demonstrates that unipolar plasticity is not a subset of bipolar plasticity, but an independent plasticity mode accessed through a different driving protocol.

Importantly, existing iontronic and memristive systems have not exhibited this unprecedented integration of voltage-driven unipolar and bipolar plasticity within a single device, with these two polarity modes typically realized in different systems. For example, Robin et al. (*Science* **379**, 161-167 (2023)) reported unipolar ion switching in MoS_2 channel-based systems and bipolar switching in activated carbon channel-based systems, highlighting that these two polarity modes arise from distinct material platforms with different interfacial and transport characteristics, rather than being integrated

within a single device architecture. In contrast, in the GIT system, both unipolar and bipolar plasticity can be realized within the same material platform by simply tuning the driving voltage amplitude, without altering the material composition or device structure. This voltage-strength-dependent polarity switching originates from distinct heterointerface-trap dynamics activated under different electric field. Therefore, explicitly differentiating unipolar and bipolar plasticity is essential for accurately describing the multistate neuromorphic behaviors uniquely enabled by the GIT architecture.

Comment 2-10: *The ultra-low energy consumption (0.61 pJ/spike) is an important claim of the authors. However, how is this defined? Is there a standard for the minimum weight change required for a single spike? Or how many spikes does the GIT need to achieve the maximal weight change? Basically, I assume the smaller the weight change per spike, the less energy it needs per spike. Moreover, how is the weight measured? What is the impedance of the total device? Will that affect energy consumption?*

Response: We sincerely thank the reviewer for this helpful and important comment regarding the definition and evaluation of the ultra-low energy consumption. The reported value of 0.61 pJ/spike is defined as the minimum energy consumption by the $GIT_{Ca/Al}$ system during the application of a paired pulse, calculated as $W=Vit$, where the minimum spike voltage V (40 mV), the minimum postsynaptic ionic current I (0.152 nA), and the pulse duration t (0.1 s) are experimentally measured under fixed conditions. And the synaptic weight is defined as the device conductance, extracted from the postsynaptic ionic current measured at a given read voltage ($G = i / V$). Regarding the correlation between the definition of energy consumption and synaptic weight change, we note that there is no universally accepted standard in the neuromorphic or iontronic literature that specifies a minimum weight change required for a single spike. In response to the reviewer's concern, we think that the minimum postsynaptic ionic current and spike voltage associated with the minimum synaptic weight change can be directly used to calculate the minimum energy consumption per spike.

Regarding the number of spikes required to reach the maximal synaptic weight change, under the same testing conditions, the GIT system reaches its saturated conductance state after > 350 consecutive programming spikes. This gradual evolution reflects the progressive accumulation of cascade-heterointerface traps rather than an abrupt conductance transition, which is consistent with the multistate neuromorphic behavior of the system. Due to the presence of cascade-heterointerface-traps, the GIT does not behave as a simple ohmic resistor, and a single, well-defined total device impedance cannot be unambiguously extracted. Instead, we characterize the device using its original ionic

conductivity, which is measured to be approximately 7.64 mS/cm under the same electrolyte and testing conditions. The device impedance (or equivalently, the current response) does affect the numerical value of the energy consumption per spike, since the energy is calculated from the measured *Vit* response during each pulse. However, in this work, the reported energy consumption is obtained directly from the experimentally measured current under fixed spike conditions, rather than from an assumed impedance value. Therefore, the influence of impedance on energy consumption is inherently included in the experimental evaluation.

3. Biological experiments

The biological experiments are amazing. However, many questions exist, such as why use $GIT_{Ca/Al}$ *not other ions? Why does the device have two channels and 4 electrodes? Biocompatibility issues. What happened at the biointerfaces? What endogenous neural signals are involved? These questions are important and worth further work (another paper) to fully explain. Therefore, I strongly recommend removing the bioapplication and only focusing on the memristive application.*

Response: We are grateful to the reviewer for the positive evaluation of the biological experiments and for raising these important questions. In our biological experiments, we demonstrate differentiated neuromorphic behaviors based on distinct ionic configurations of the GIT system, including $GIT_{Ca/Al}$, $GIT_{Cl/ClO}$, and GIT_{Ca}, and construct an *in vivo* GIT-based neuro-iontronic processor to realize interneural signal reconfiguration and plasticity modulation (***Figs. 4a-4b***). As shown in ***Fig. 4***, the *in vivo* neuro-iontronic processor is implemented in a dual-channel and four-electrode architecture, in which two GIT channels are integrated in parallel and connected to the proximal and distal sciatic nerve segments through electrodes, enabling potentiation and depression neuromorphic processing. When driven by identical endogenous neural spike potentials from the proximal nerve interface, the $GIT_{Ca/Al}$ and $GIT_{Cl/ClO}$ channels sequentially exhibit downstream neural signal reconstruction and plasticity modulation (***Figs. 4c-4e***). Specifically, corresponding to the results in ***Fig. 3***, the GIT_{Ca} with weaker heterointerface-trap strength than that of $GIT_{Ca/Al}$, reconstructs downstream signals at the distal sciatic nerve that closely match the original neural signals, while $GIT_{Ca/Al}$ could enhance this signal (***Fig. 4c and Supplementary Fig. 37***). Meanwhile, the $GIT_{Cl/ClO}$ channel displays neuromorphic temporal plasticity depression behavior, resulting in suppressed downstream neural signal responses under the same endogenous neural input conditions (***Fig. 4e***). In this case, the cascaded-heterointerface-trap mechanism is driven by upstream endogenous neural signals, enabling interneural signal

reconfiguration and plasticity modulation. Furthermore, the channel dimensions used for biological integration are kept identical to those employed in the ionic rectification and memristive characterization, ensuring consistent demonstration of testing and functionality (***Figs. 2-3***). As designed in the device architecture, each GIT channel is interfaced with neural tissue via four PEDOT:PSS hydrogel electrodes, owing to their low impedance, conformal contact, and excellent mechanical and electrical compatibility with neural tissue, which minimizes tissue damage and ensures reliable transmission of endogenous biopotentials (***Fig. 4a***).

At the biointerfaces, we construct a functional biohybrid neural circuit by integrating the *in vivo* neuro-iontronic processor between the proximal (upstream) and distal (downstream) segments of the transected sciatic nerve via four PEDOT:PSS hydrogel electrodes. This configuration enables direct coupling between neural tissue and the iontronic processor without applying any external electrical stimulation. The *in vivo* neuro-iontronic processor with intrinsic signal transduction and processing capabilities can be embedded within the sciatic neural pathway, actively modulating bioelectrical signals originating from the upstream nerve segment and relaying the processed output to the downstream nerve terminals. Upstream neural activity generates extracellular bioelectrical activity that serves as input biopotential signals to the GIT processor, further activating heterointerface-trap dynamics and producing neuromorphic ionic currents. Thus, these neuromorphic signals can in turn modulate the distal nerve interface to facilitate and trigger action potentials in the downstream nerve. The endogenous neural signals involved are the upstream neural signals, downstream neural signals and reconstructed downstream neural signals of the sciatic nerve, evoked by a well-established rhythmic tail-pinch protocol in rodent models. This protocol reliably generates sensory afferent signals transmitted from the tail to the spinal cord and relayed to the sciatic nerve. From an electronic-circuit perspective, the biohybrid system functions analogously to an endogenous-signal-driven memristive circuit, in which upstream neural biopotentials serve as the input, the GIT materials with cascaded-heterointerface-traps provide the neuromorphic processing functions and the modulated ionic currents constitute the output delivered to the downstream nerve. Electrophysiological recordings confirm that original (pre-transection) and upstream (post-transection) neural spike signals are equivalent and serve as baseline references. Control experiments performed after nerve transection without the GIT processor yielded no detectable downstream neural responses, confirming that signal transmission across the transected nerve depends entirely on the functional integration of the GIT device. Upon introducing the GIT processor, reconstructed downstream neural signals reappear with clear temporal

correlation to the stimulation and exhibit neuromorphic excitatory or inhibitory plasticity. Concurrent electromyographic (EMG) recordings further verify that these downstream biopotentials correspond to functionally relevant neuromuscular activation.

Following the reviewer's suggestion, we further conduct comprehensive biocompatibility assessments at the cellular and tissue levels. The *in vitro* cytotoxic evaluation of GIT samples is assessed by the live/dead staining assays and the CCK-8 test. Herein, live/dead staining and CCK-8 assays are performed to assess the viability of cells co-cultured with the GIT and to evaluate its cytotoxicity. As displayed in ***Fig. R8*** ***(Supplementary Fig. 34)***, following 7 days of incubation, the morphology of live HT22 cells in the hydrogel group is comparable to that in the control group. Accordingly, almost no dead cells are detected in either the control or hydrogel group. Consistent results are obtained from the CCK-8 assay, where the viability of HT22 cells cultured with the GIT remains close to the control group. Collectively, these results confirm that the as-prepared hydrogel possesses excellent cytocompatibility. The hematoxylin and eosin (H&E) staining is performed on the major organs of rats, including the kidney, spleen, and liver, to systematically evaluate the *in vivo* biocompatibility of the gel material, and the results are compared with those of the sham-operated control group. As shown in ***Fig. R9*** ***(Supplementary Fig. 35)***, no obvious inflammatory cell infiltration, tissue necrosis, or structural damage is observed in the kidney, spleen, or liver of either the gel-implanted group or the sham control group. In the kidney, the glomerular and tubular structures remain intact and well-organized, with no significant inflammatory response in the renal interstitium. The spleen maintains a normal histological architecture with clearly defined white and red pulp regions, and no excessive lymphocyte proliferation or hemorrhage is detected. The liver tissue exhibits a typical lobular structure, with orderly arrangement of hepatocytes and normal cellular morphology. Collectively, these findings demonstrate that the gel material possesses excellent tissue biocompatibility, as it does not induce significant adverse histological changes in vital organs, indicating its high safety profile for *in vivo* biomedical applications. The corresponding results have been added to the ***Supplementary Figs. 34-35***, and discussion have been included in revised manuscript.

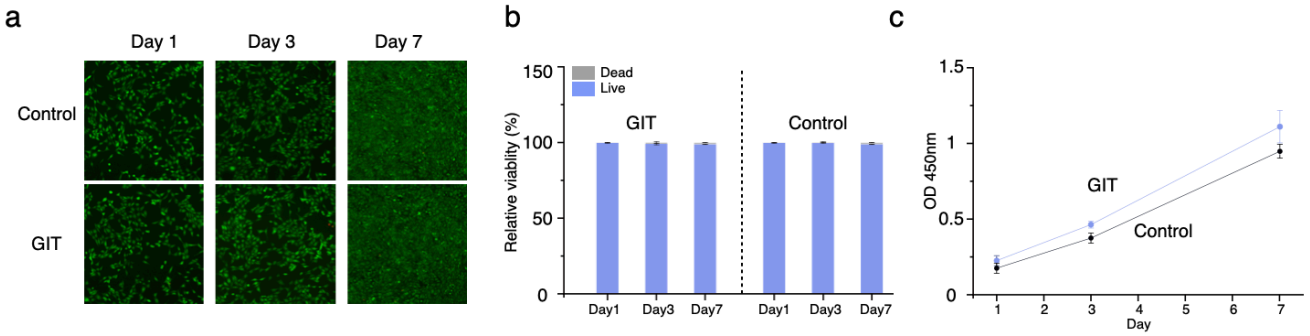

Fig. R8 ***(new Supplementary Fig. 34)*** *Live/dead fluorescence staining images show the changes in cell state on days 1, 3, and 7 of culture in the control and GIT-treated groups. Green fluorescence represents surviving cells. Both groups of cells exhibited good viability and continuous proliferation throughout the culture period, with cell density increasing significantly over time, forming a dense cell layer by day 7. Compared with the control group, no significant cytotoxicity or proliferation inhibition was observed in the GIT -treated group, indicating that the GIT system has good biocompatibility.*

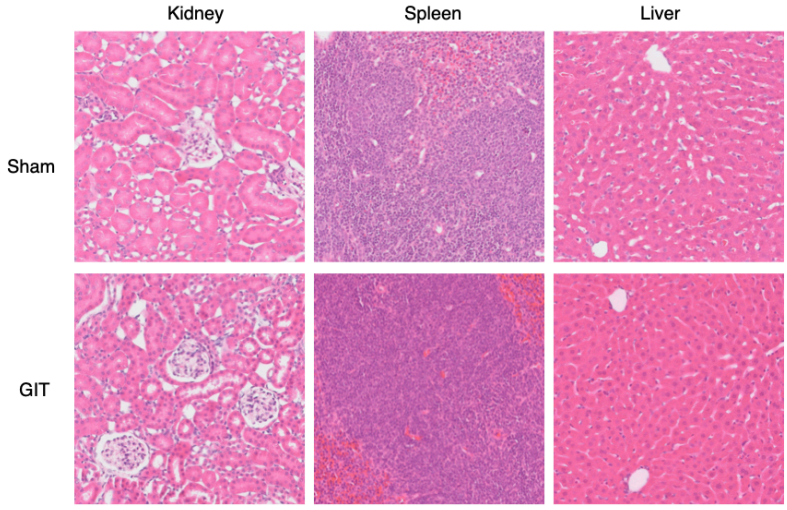

Fig. R9 ***(new Supplementary Fig. 35)*** *Representative H&E staining images of major organs (kidney, spleen, and liver) from rats in the sham-operated control group (Sham) and the gel-implanted group (GIT). Scale bar:100μm. n=6.*

4.1 The authors should briefly explain how to use GITs as modular components, the miniaturization, and how to integrate them into iontronic systems.

Response: We appreciate the reviewer for this comment. In this work, GITs, as a soft-matter iontronic materials, are designed and utilized as modular iontronic components, enabling straightforward integration into functional iontronic and biohybrid systems. Specifically, the biohybrid neural circuit is

constructed by physically interfacing a GIT-based neuro-iontronic processor (1.5 mm × 250 μm × 100 μm per channel) with the transected sciatic nerve of anesthetized rats via 3D-printed PEDOT:PSS hydrogel bioneural electrodes (1 mm × 100 μm × 100 μm). Importantly, all GIT channels used for system-level integration adopt the same chemical composition and microscale geometry as those used in the ionic rectification, memristive, and neuromorphic characterization. This ensures consistent demonstration of testing and functionality for ionic rectification, memristive, and neuromorphic behaviors. As a soft-matter iontronic material, the GITs inherently support modular integration, allowing different GIT channels to be configured with distinct ionic species to realize differentiated neuromorphic functions. This modularity enables future multi-channel GIT architectures for endogenous neural signal processing, providing a scalable platform for artificial neural interfaces, smart sensors, and ionic biohybrid computing frameworks.

4.2 Microfont in Fig. 4b. Time is unclear in SI Fig. 5. SI Fig. 15 is unclear. Can a single-sided GIT achieve a memristive effect? f Data in SI Fig. 19 is missing.

Response: We thank the reviewer for pointing out these issues. We have revised ***Fig. 4b*** by enlarging the microfont for improved readability, clarified the time annotation in ***Supplementary Fig. 5 (New Supplementary Fig. 8)***, and improved the clarity of ***Supplementary Fig. 15***. Specifically, the time in the revised ***Supplementary Fig. 8*** represents the duration of the applied forward electric field ranging from 0 to 5 s in the MD simulation of ion cross-interface transmission, and this has now been explicitly stated in the figure caption. For the revised ***Supplementary Fig. 15***, we have revised the caption to clearly indicate that the AEP sub-heterointerface represents the polyanion electrolyte heterogel component of the GIT system, while the CEP sub-heterointerface corresponds to the polycation electrolyte heterogel component. We would like to clarify that the data in ***Supplementary Fig. 19*** are not missing. According to the calculation of the reverse rectification ratio ($f' = -|-i_{max}/+i_{max}|$), the bilayer polyelectrolyte hydrogel exhibits negligible rectification, as the $-i_{max}$ approaches zero, resulting in a rectification ratio close to zero. Following the reviewer's suggestion, we further provide memristive measurements of the AEP sub-heterointerface and the CEP sub-heterointerface. As shown in ***Fig. R16***, the single heterointerface exhibits only limited ion accumulation and fails to produce memristive behavior. This is because, in the absence of electrostatic partitioning and cascaded-heterointerface coupling, single-sided structures cannot establish the heterointerface-trap dynamics. This result highlights the necessity of the complete cascaded-heterointerface architecture.

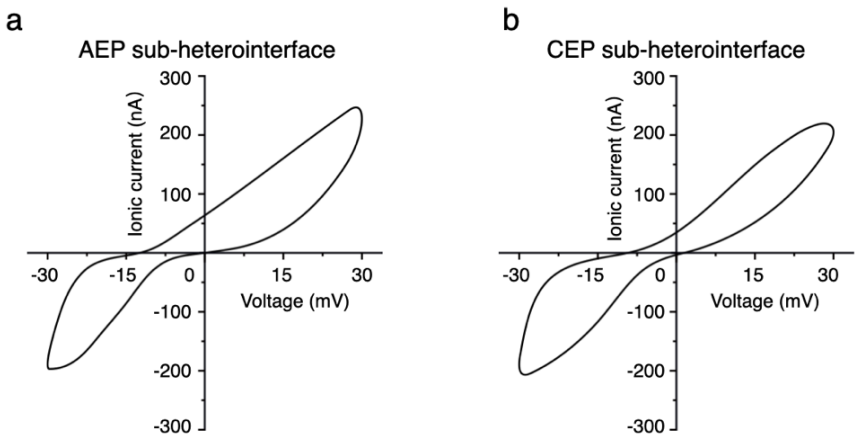

Fig. R16 *I-V curves of the AEP sub-heterointerface (a) and the CEP sub-heterointerface (b). AEP sub-heterointerface and CEP sub-heterointerface denote the polyanion and polycation electrolyte heterogel components of the GIT system, respectively.*

In conclusion, we sincerely appreciate the reviewers for their thoughtful and constructive feedback. We have thoroughly revised the manuscript and Supporting Information to clarify key mechanisms, strengthen experimental details, and improve the overall discussion. In response to the reviewers' comments, we have added new data and analysis on the heterointerface ion-trap mechanism and ionic rectification, as well as biocompatibility results. We hope these revisions address the reviewers' concerns and enhance the overall quality of the manuscript.

Responses to Referees' Comments

Reviewer 1

In the revised version of the manuscript, the authors addressed most of my comments. I believe that in this form, the manuscript id suitable for publication in Nature Electronics.

Response: We sincerely thank the reviewer for the positive evaluation of our revised manuscript. We are very pleased that the reviewer considers that most comments have been adequately addressed and that the manuscript is now suitable for publication in Nature Electronics. We deeply appreciate the reviewer's thoughtful and constructive feedback, which has significantly helped us improve the rigor, clarity, and presentation of this work.

Reviewer 2

The authors have addressed my comments in a very complete manner. They havep rovided additional data where required, modified Figures, and enhanced parts of the discussion. I recommend acceptance for publication of this work in Nature Electronics.

Response: We sincerely appreciate the reviewer for the positive evaluation of our manuscript, including the recognition of its novelty, structural clarity, and relevance to the field of iontronic neuromorphic systems. Your comments have helped us further improve the manuscript. Detailed point-by-point responses are provided below.

1. Related to Figure 4, the definition and importance of interfacing biology with iontronic devices (bioiontronics) should be further discussed.

Response: We thank the reviewer for this insightful comment. In the revised manuscript, we have added further discussion in the section "Bioneuron-driven ionic neuromorphic processing" to clarify the definition and significance of bioiontronics, as follows: "These results demonstrate that our GIT-based neuro-iontronic processors possess the capability to be driven directly by endogenous biological neural potentials, effectively obviating the need for external power sources or supplementary electrical signals. By executing neuromorphic processing, these processors achieve the effective restoration of downstream neural biopotentials and dynamic plasticity modulation. Such promising integration establishes a foundational closed-loop paradigm for bioiontronics, utilizing ions as neuromorphic information carriers to bridge the iontronic signaling gap within abiotic-biotic systems."

2. Small fonts still exist in some main Figures.

Response: We thank the reviewer for pointing this out. In the revised manuscript, we have enlarged the small fonts in in Fig. 3e, f and Fig. 4b, c to improve readability and adjusted the layout where necessary to ensure that all annotations remain clear.

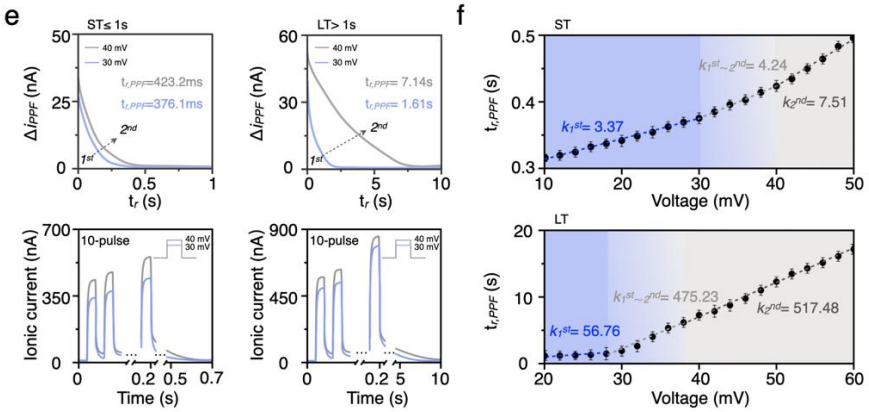

Fig. 3: Multistate ionic neuromorphics.

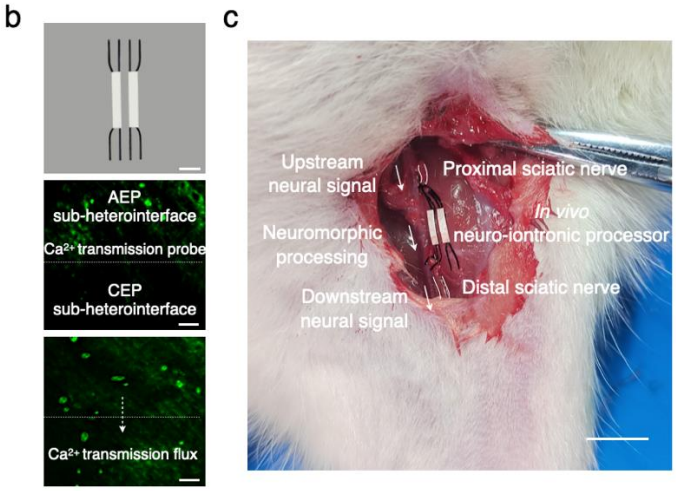

Fig. 4: Bioneuron-driven ionic neuromorphic processing.

Reviewer comments:

In this paper, Wu et al. developed a unique iontronic device, termed the gel-multiphasic ion transporter (GIT), which demonstrated outstanding ionic memristive effects and operated at biointerfaces as a bioiontronic device for neuromorphic processing (neural signal transmission). The work is an interesting extension of their previous work (***Science*** 382, 559-565 (2023)), which elegantly used a cascade-heterogated biphasic gel (HBG) for ion selection and the modulation of biological activity. Here, the authors applied the HBG principles to the development of the GIT, which, in my opinion, is fundamentally a bipolar membrane heterojunction, i.e., an iontronic diode. Many iontronic diodes have been reported previously. However, the HBG structure in this work introduced new, intriguing properties to the field, including memristive effects, low energy consumption, and ion specificity. Further, the last biological application is mind-blowing (I will mention the problem with it later). Therefore, I appreciate the authors' endeavour and believe this work has significant potential impact. However, some major issues need to be addressed before acceptance.

Major issues:

1. Writing issue:

The ionic mechanism of the GIT is very obscure and difficult to understand. The writing in Sections 'Cascade-heterointerface-trap ion transmission' and 'Bidirectional ionic rectification' is abstruse and mouthful, and Figs. 1 to 3 are not clear for the mechanism explanation. Below are my detailed comments.

1.1 I understand the strong connection and breakthrough between this work and the previous HBG paper. However, not every reader is aware of the HBG, and Figure 1 does not clearly present basic information about the GIT. What are the material compositions of the HBG? How does an actual device look? Some information in the SI should be put there, or an extended data Figure at least. And virtual photos of the device should be presented.

1.2 I would remove the long paragraph in Section 'Cascade-heterointerface-trap ion transmission', starting from 'The heterointerface architectures established ionic cross-interface transfer energy barriers (ΔE)…' to the end of the paragraph. The content here serves as an introduction, but it largely overlaps with the information in the abstract without giving any new information. Further, the many compound words/terms are difficult to read, failing to convey the meanings behind.

1.3 The awkward terms include 'ionic cross-interface transfer energy barriers', 'cascade-heterointerface-traps governed ionic nonlinear transmission', 'asymmetric central interfacial charge accumulation', 'spike-strength/timing dependent dual-order (i.e., unipolar and bipolar) plasticity features', etc.

1.4 I strongly recommend replotting Fig. 1b to 1e to first divide the CV scan into multiple steps/regions and correlate the mechanistic schematics (1b) aside to give explanations. The same for Fig. 3a to c.

1.5 Many terms used in this manuscript are also misleading. 'bidirectional ionic rectification'

does not make sense to me. Rectification in the context of iontronics means that only one direction of ionic current can pass, i.e., it behaves as a diode. The ‘bidirectional’ nullifies this term. Also, the same effect has been widely observed in biological nanopores and correlated dropletronic memristive devices (DOI: 10.1039/d5cs00580a). The authors should mention this and provide a discussion.

1.6 The term ‘neuromorphic’ has also been widely used in this manuscript. However, its meaning is imprecise. ‘Memristive’ is a better and more accepted replacement.

1.7 The paragraph that starts with ‘As illustrated in Fig. 1b and Supplementary Fig. 2…’ is essential but difficult to read. I strongly recommend a rewrite with clear words and shorter sentences.

2. Mechanisms:

My understanding of the GIT is that it comprises two oppositely charged HBGs and forms an iontronic diode structure. In addition to conventional iontronic diodes, the unique structure of the HBGs induces a significant capacitance effect at the center heterointerface, so-called the relay medium phase (RMP), which results in the memristive feature.

2.1 I don’t understand why ΔEn > … > ΔE2 > ΔE1. The HBG is evenly distributed, and the cross-interface transfer energy barriers should be the same. Of course, their accumulation cascades, e.g., the working mechanism of HBG.

2.2 ‘Initially, AEP acted as a cation- and anion-enriched phase, while CEP contained free anions.’ What do you mean? Shouldn’t AEP only contain free cations?

2.3 The calculation of forward (f) and reverse (f’) rectification ratios is unclear. The methods used in conventional iontronic diodes should be considered, and the performance under alternating voltages should be measured.

2.4 The influence of frequency and scanning rates should be further explained in the rectification section, and clearly shown in the Figures.

2.5 The part ‘The GIT material was fabricated through a…’ should be moved to the beginning.

2.6 The influence of various ion species is important. Could the authors try protons?

2.7 The mechanism of ion concentration is unclear. The results in SI Fig. 16 seem to show that higher ion concentration shows higher ion rectification, which is contradictory to the explanation in the main text.

2.8 The hydrogel materials (bilayer polyelectrolyte hydrogelCa/Al) should be clearly explained. Different hydrogel materials may provide different performances.

2.9 I don’t understand the need to differentiate the unipolar and bipolar plasticity features. Isn’t the unipolar state a part of the bipolar state?

2.10 The ultra-low energy consumption (0.61 pJ/spike) is an important claim of the authors. However, how is this defined? Is there a standard for the minimum weight change required for a single spike? Or how many spikes does the GIT need to achieve the maximal weight change? Basically, I assume the smaller the weight change per spike, the less energy it needs per spike.

Moreover, how is the weight measured? What is the impedance of the total device? Will that affect energy consumption?

3. Biological experiments

The biological experiments are amazing. However, many questions exist, such as why use GITCa/Al not other ions? Why does the device have two channels and 4 electrodes? Biocompatibility issues. What happened at the biointerfaces? What endogenous neural signals are involved? These questions are important and worth further work (another paper) to fully explain. Therefore, I strongly recommend removing the bioapplication and only focusing on the memristive application.

4 Other issues

4.1 The authors should briefly explain how to use GITs as modular components, the miniaturisation, and how to integrate them into iontronic systems.

4.2 Microfont in Fig. 4b. Time is unclear in SI Fig. 5. SI Fig. 15 is unclear. Can a single-sided GIT achieve a memristive effect? f Data in SI Fig. 19 is missing.